Palaeogeography, Palaeoclimatology, Palaeoecology 477 (2017) 40–54

Contents lists available at ScienceDirect

Palaeogeography, Palaeoclimatology, Palaeoecology

journal homepage: www.elsevier.com/locate/palaeo

Intermittent euxinia in the high-latitude James Ross Basin during the latest Cretaceous and earliest Paleocene

Shane D. Schoepfer [a,*], Thomas S. Tobin [b], James D. Witts [c,d], Robert J. Newton [c]

[a] Department of Geoscience, University of Calgary, Calgary, AB, Canada
[b] Department of Geological Sciences, University of Alabama, AL, USA
[c] Earth Surface Science Institute, School of Earth and Environment, University of Leeds, UK
[d] Division of Paleontology (Invertebrates), American Museum of Natural History, NY, USA

ARTICLE INFO

Article history:
Received 14 January 2017
Received in revised form 15 April 2017
Accepted 15 April 2017
Available online 19 April 2017

Keywords:
Anoxia
Extinction
Antarctica
Seymour Island
Glauconite

ABSTRACT

Seymour Island, in the James Ross Basin, Antarctica, contains a continuous succession of latest Cretaceous sediments deposited in a shallow marine environment at high latitude, making it an ideal place to study environmental changes prior to the K–Pg mass extinction. We measured major and trace elements and conducted petrographic analysis of two sections from the Maastrichtian–Danian López de Bertodano Formation of Seymour Island. Several lines of evidence point to intermittently anoxic to euxinic conditions during deposition, including the presence of pyrite framboids with a size distribution suggesting syngenetic formation in the water column, and enrichments in several trace elements, including molybdenum, arsenic, copper, zinc, and chromium. Molybdenum enrichments are clearly associated with enrichments in manganese and authigenic iron, suggesting "shuttling" of redox sensitive trace elements across a chemocline that fluctuated across the sediment-water interface. Comparisons with modern systems suggest relatively high-frequency redox variability, possibly over approximately annual timescales, which may be related to the annual cycle of polar sunlight and associated seasonal changes in primary productivity. Glauconitic horizons are associated with more reducing conditions, including at the K–Pg boundary, though this does not appear to be a uniquely euxinic interval; similar degrees of trace element enrichment are seen in other highly glauconitic intervals. While euxinia may have contributed to low diversity in the lowermost '*Rotularia* Units', redox conditions do not seem to have been the primary control on the transition to a mollusc dominated fauna in the latest Maastrichtian. Redox conditions show little to no response to the eruption of the Deccan Traps or Maastrichtian climatic changes. Instead, intermittent euxinia appears to have been a characteristic feature of this high-latitude environment during the Cretaceous–Paleogene transition.

1. Introduction

The Cretaceous-Paleogene (K–Pg) mass extinction was among the most severe biodiversity crises of the Phanerozoic, ending the Mesozoic Era and impacting both marine and terrestrial flora and fauna on a global scale. The Chicxulub extraterrestrial impact has been firmly linked to the K–Pg extinction worldwide (Schulte et al., 2010). However, the extinction event also occurred during a period of longer-term environmental change. Several lines of evidence suggest that the Mesozoic and early Cenozoic were characterized by a greater degree of environmental variability than is typically implied when they are described as stable 'greenhouse' environments (Clarke and Jenkyns, 1999; Miller et al., 2005; Friedrich et al., 2012). Global temperatures reached a minimum during the Maastrichtian stage (72–66 Ma; Linnert et al., 2014), alongside evidence for large and rapid sea level changes (Miller et al., 2005).

In addition, the terminal Maastrichtian also saw the eruption of the extensive Deccan Traps large igneous province (LIP) in India (Schoene et al., 2015; Renne et al., 2015). Given the prominent role that LIPs are believed to have played in driving environmental changes during other mass extinction events (Wignall, 2001; Bond and Wignall, 2014), it is reasonable to ask whether cascading environmental impacts of the Deccan Traps eruptions on a global scale could have contributed to the end-Cretaceous extinction event (Caldeira and Rampino, 1990; Kidder and Worsley, 2010; Courtillot and Fluteau, 2010; Tobin et al., 2016).

These differing explanations for the cause of the K–Pg extinction need not be mutually exclusive. A "press-pulse" model, in which mounting long-term environmental stress is punctuated by a catastrophic event, has been proposed as a general model for mass extinctions (Arens and West, 2008). Fully assessing the applicability of this

* Corresponding author.
E-mail address: shane.schoepfer@ucalgary.ca (S.D. Schoepfer).

http://dx.doi.org/10.1016/j.palaeo.2017.04.013

model to the terminal Cretaceous requires a detailed understanding of potential environmental deterioration leading up the extinction horizon. Changes in temperature resulting from Cretaceous climate evolution or the Deccan Traps eruptions and associated greenhouse gases may have been especially prevalent in the environmentally sensitive high latitudes (Tobin et al., 2012; Petersen et al., 2016).

Our understanding of high-latitude environments during the Cretaceous–Paleogene 'greenhouse' remains poor, even in their "baseline" state prior to the environmental disruptions of the K–Pg mass extinction. There is no modern analogue for these settings (Chin et al., 2008), which were characterized by extensive vegetation cover and a lack of large permanent ice sheets on land, but were governed by the extreme seasonality of the polar light regime. Records from high-latitude Cretaceous environments have the potential to yield important clues about the sensitivity of polar ecosystems to warm climates in the near-future (e.g. Davies et al., 2009).

Seymour Island (SI), in the James Ross Basin, Antarctica (Fig. 1), contains the southernmost, most expanded onshore K–Pg succession in the Southern Hemisphere, and has been the subject of intense paleontological and geochemical study (e.g. Feldmann and Woodburne, 1988; Crame et al., 2004; Olivero, 2012). In this study, we aim to: 1) characterize pre-extinction "baseline" redox conditions in the James Ross Basin during the latest Cretaceous and early Paleocene using new petrographic and geochemical data; 2) determine whether changes in basinal redox chemistry can be linked to local and/or global environmental changes; and 3) assess the effects of any such redox variability on the local marine fauna, prior to and during the K–Pg mass extinction.

2. Geologic setting

2.1. Overview

Extensive outcrops of Early Cretaceous to Eocene sediments deposited in the James Ross Basin (JRB) are exposed across an archipelago of islands located off the northeastern tip of the Antarctic Peninsula (Fig. 1). Despite its relative inaccessibility, the JRB has received intermittent study since the early 20th century (e.g., Kilian and Reboul, 1909; Spath, 1953; Wilckens, 1910), as it provides the key nearshore sedimentary succession of this age in Antarctica. Deposition occurred in a rapidly subsiding back-arc basin to the east of the Antarctic Peninsula magmatic arc (Elliot, 1988; Hathway, 2000), and the Mesozoic basin-fill is typically divided into two principal lithostratigraphic groups: the 2.6 km-thick Gustav Group (Barremian-Coniacian; Riding and Crame, 2002; Crame et al., 2006), overlain by the 3 km-thick Marambio Group (Santonian-Danian; Rinaldi et al., 1978; Crame et al., 1991; Olivero, 2012).

Much of the JRB sedimentary succession, particularly in the Marambio Group, is highly fossiliferous (Feldmann and Woodburne, 1988 and references therein; Pirrie et al., 1997; Crame et al., 2004), and the fossils are generally quite well-preserved, both physically and geochemically (Ditchfield et al., 1994; Dutton et al., 2007; Tobin et al., 2012; Tobin and Ward, 2015). The excellent preservation of fossil material, and the poor consolidation of the sediments, are largely the consequences of minimal burial depth and a lack of tectonic activity in the area since deposition. There has been little tectonic movement of the

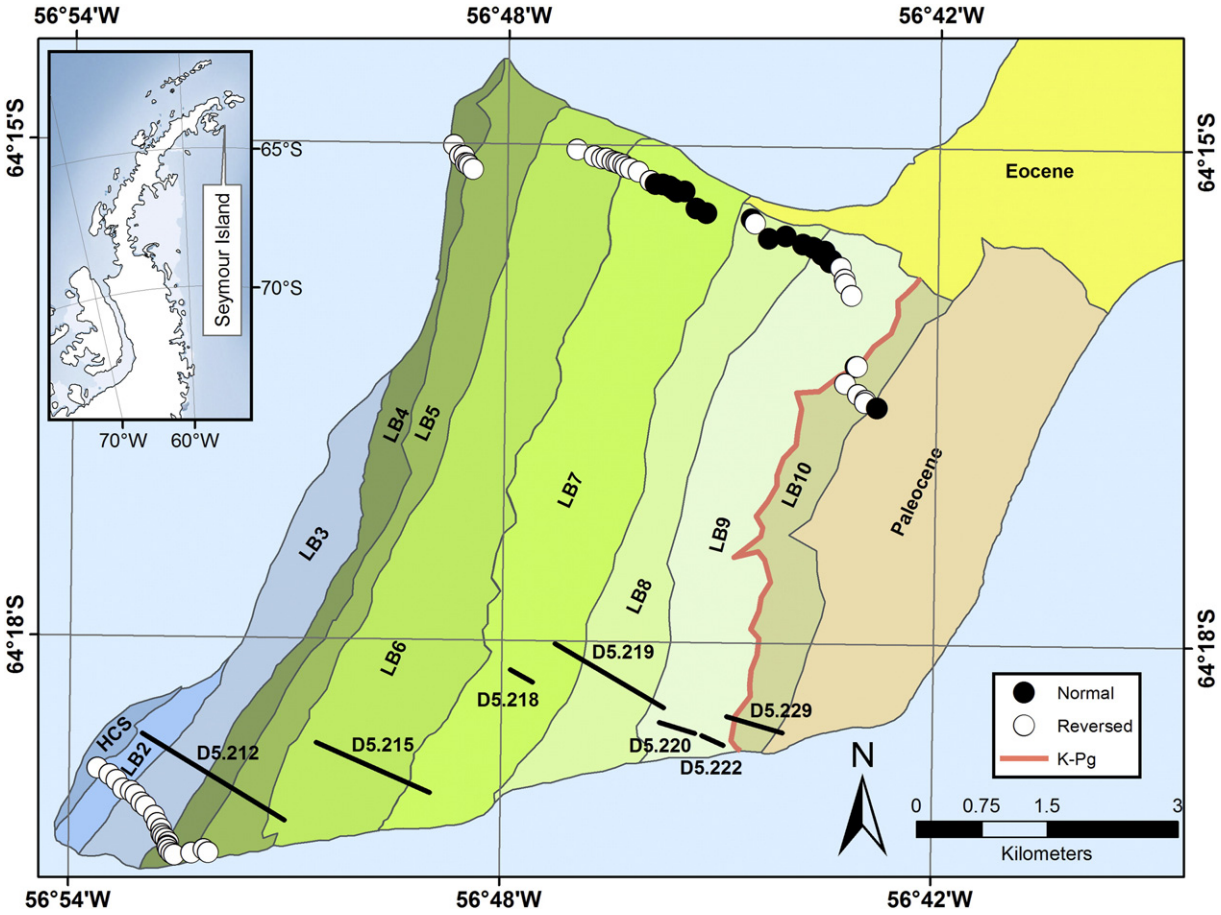

Fig. 1. Simplified geologic map of Cretaceous–Paleogene strata on Seymour Island (after Montes et al., 2013). LBX indicates the informal units of the Lopez de Bertodano Fm. (Macellari, 1988). HCS = Haslum Crag Sandstone. Black and white dots indicate locations of paleomagnetically normal and reversed samples from the T12 section, D5.2XX are schematic subsections of the BAS section trace.

JRB since the Cretaceous and Paleocene, and the latitude of the basin at the time of deposition is reconstructed as being within 1–2° of its present-day location (Lawver et al., 1992; Tobin et al., 2012).

The Campanian through Danian sedimentary succession has experienced only minor faulting, and has a shallow and roughly uniform dip of ~8–12° to the ESE. Beds dip more steeply in the older strata (Crame et al., 2006), which is most likely a consequence of continued subsidence and compaction rather than significant tectonic compression (Hathway, 2000). Later eruption of a Neogene volcanic complex (Smellie et al., 2008) has topped many of the islands with basalt flows and pyroclastic deltas, which serve to stabilize the poorly indurated underlying sediments, though occasional cross-cutting feeder dikes can locally alter the sediment. The JRB sediments have only experienced burial to depths <2 km, at low pressures and temperatures likely insufficient to produce significant diagenesis (Askin and Jacobson, 1989; Svojtka et al., 2009; Tobin et al., 2012).

2.2. Stratigraphy

This study focuses on the ~1100 m-thick López de Bertodano Formation (LBF) on SI, which forms the majority of the upper portion of the Marambio Group throughout the basin (Pirrie et al., 1997; McArthur et al., 2000; Olivero, 2012). The LBF on SI is composed of fairly monotonous sandy to clayey siltstones, with occasional well-cemented sandier layers, some of which contain post-depositional carbonate concretions. A number of discrete beds throughout the succession also contain significant amounts of glauconite (Macellari, 1988; Crame et al., 2004; Bowman et al., 2013). Primary depositional textures are often obscured by freeze-thaw weathering of the surface, and in places by apparently extensive bioturbation, and primary sedimentary fabrics have never been studied systematically (though see Olivero et al., 2007; Olivero et al., 2008). Fine-scale variability in grain-size and sedimentary architecture has been described, particularly in the lower portion of the LBF (Olivero et al., 2007; Olivero et al., 2008) which can probably be related to local water-depth changes.

Macellari (1988) used biostratigraphic and lithostratigraphic constraints to identify a series of informal units in the LBF on Seymour Island; the lower '*Rotularia* Units' (here numbered LB1–6) and the upper 'Molluscan Units' (here numbered LB7–10) are named after their characteristic macrofossils. The 'Molluscan Units' are extremely fossiliferous, especially Units LB9 and LB10, which straddle the K–Pg boundary (Macellari, 1988; Elliot et al., 1994; Zinsmeister, 1998). Unit LB1 of the '*Rotularia* Units' was subsequently reassigned to the underlying Haslum Crag Member of the Snow Hill Island Formation (SHIF; Pirrie et al., 1997; Crame et al., 2004, Olivero, 2012) and is capped by a prominent unconformity (Olivero et al., 2007, 2008). The portion of the SI succession assigned to the '*Rotularia* Units' contains clear lateral facies variation and large channel structures, which further complicates the stratigraphy on a small scale (Olivero, 1998; Olivero et al., 2007; Montes et al., 2013).

Due to the various difficulties outlined above and the apparent lithological homogeneity of much of the succession, these informal units can be difficult to recognize in the field, and in many studies the LBF is not subdivided (e.g., Crame et al., 2004; Bowman et al., 2012; Witts et al., 2016). However, the subdivisions are differentiated in published geological maps (e.g., Montes et al., 2013), meaning that their boundaries, along with other features such as the K–Pg boundary and several distinctive glauconite-rich horizons, can be used to attempt correlation between sets of samples collected by different workers (e.g., Bowman et al., 2013; Witts et al., 2016, Section 2.4).

A robust age model has been developed for the LBF based on biostratigraphy (Macellari, 1986; Huber, 1988; Bowman et al., 2012; Witts et al., 2015), chemostratigraphy (primarily strontium isotopes; McArthur et al., 1998), and magnetostratigraphy (Tobin et al., 2012), as well as the presence of an iridium (Ir) anomaly at the K–Pg boundary (Elliot et al., 1994; see Witts et al., 2016 for more details). This has confirmed the Maastrichtian–Danian age of the succession, and also the high rate of sedimentation during the Cretaceous-Paleogene interval (10–20 cm/kyr), with the entire sequence on SI likely deposited in <4 million years (Tobin et al., 2012; Bowman et al., 2013). The homogenous nature of these deposits, and the lack of significant grain size variation or evidence for significant hiatuses, suggests essentially continuous sedimentation.

2.3. Depositional environments

The Santonian through Danian succession in the JRB is generally interpreted to have been deposited in shallow marine (largely open) shelf environments (Macellari, 1988; Olivero, 2012), with water depth and sedimentary architecture affected by a combination of global sea level and local tectonic controls (Olivero et al., 2008). On SI, the LBF was deposited on a prominent lowstand erosion surface that cuts down as much as 60 m into the underlying SHIF (Olivero et al., 2007, 2008). The lower portion of the LBF succession (assigned to the '*Rotularia*' Units) contains a fossil assemblage dominated by calcareous tubes of the serpulid *Rotularia*, with other macrofossils rare or absent. Based on the fossil fauna and sedimentology, this interval is believed to represent estuarine deposition in a large, relatively shallow embayment, during a period of overall transgression (Olivero et al., 2007, 2008).

The superjacent 'Molluscan Units' represent a generally deepening upwards trend, with Macellari (1988) suggesting a transition from middle (Units LB7–8) to outer (Units LB9–10) shelf, though a short interval of regression may have occurred just prior to the K–Pg boundary (Macellari, 1988). Minor water depth changes are difficult to discern based on sedimentology or fossil assemblages (Bowman et al., 2012; Witts et al., 2015), however the 'Molluscan Units' clearly do show a marked increase in both the abundance and diversity of macrofossils (Macellari, 1988; Crame et al., 2004; Witts et al., 2016). The uppermost ~300 m of the Cretaceous succession are also characterized by an increase in the prelavence of relatively sandy, glauconitic beds, ranging from tens of cm to several meters thick. These may represent periods of slower deposition and reworking, or lateral facies variability (Bowman et al., 2016). The K–Pg boundary is located close to the base of one such unit (Zinsmeister, 1998; Witts et al., 2016).

Previous petrographic work has hinted at the presence of redox variations in this succession (Witts et al., 2016) despite the presence of a diverse marine fauna (Macellari, 1988; Crame et al., 2004). Additionally, clumped isotope estimates of water $\delta^{18}O$ may imply a measurable input of terrestrial meteoric water to the local depositional environment (Petersen et al., 2016).

2.4. Stratigraphic correlation

The samples analyzed in this study were collected from parallel sections across northern and southern Seymour Island, collected by two different research teams: a section collected by a joint Caltech and CADIC -Conicet-IAA team (hereafter the T12 section; first published in Tobin et al., 2012) and the British Antarctic Survey (BAS) composite section D5.251 (published in Bowman et al., 2013; Witts et al., 2016). While direct meter-to-meter correlation of sections collected from different parts of the island is not always possible due to the difficulties outlined above, especially in the lower portion of the sequence, correlations between sections can be established with reasonable confidence. This is demonstrated by the strong correspondence in first and last appearances of macrofossils across the island (Witts et al., 2015; Witts et al., 2016). Tobin and Ward (2015) were able to correlate historic collections to a single continuous section on the north side of the island, using stratigraphic plane analysis (Zinsmeister, 2001) and a simple linear stretch between tie points to account for thickness differences, finding good agreement in stable isotopic data between correlated locations.

We applied several approaches to correlate the two sections included in this study, including geographically correlating along strike using published geologic maps (Brecher and Tope, 1988; Montes et al., 2013), but these efforts were hampered by the topographic relief and along strike variations between units. Instead, a simple linear stretching model was applied to a portion of the BAS composite section D5.251 (1013 m, comprised of sub-sections D5.212, D5.215, D5.218, D5.219, D5.220, D5.222, and D5.229) to generate stratigraphic height measurements that correspond with those in the T12 section (1191 m – note base of section used here is at the base of Unit LB2, not LB5 as in Tobin et al., 2012). The base of LBF Unit 2 and the K–Pg boundary were used as tie points, and the BAS composite section was expanded so that its stratigraphic heights matched those of the T12 section over that interval. The stratigraphic uncertainty of this technique increases toward the middle of the section, away from the points of known correlation. This linear stretching model differed by at most 60 (stratigraphic) meters from methodologically independent attempts to directly link the BAS sections with paleomagnetic sampling localities from Tobin et al. (2012) using geologic mapping techniques.

3. Materials and methods

3.1. Major and trace element analyses

Freeze-thaw weathering is pervasive throughout the James Ross Basin, obscuring fine-scale surficial sedimentary features and potentially affecting geochemical signals. To minimize the potential impact of surficial weathering, samples from the T12 section were measured for major and trace elements in the end chips of 53 short cores originally drilled for paleomagnetic analysis to a depth of 15–20 cm (Tobin et al., 2012). These end chips were from the deepest part of the core, and were crushed and disaggregated into loose sediment samples.

For each of these samples, ~0.5 g of sediment was transferred into a Savillex 60 ml beaker, and covered with a solution of HNO_3, HF, and $HClO_4$ (10 ml each). Beakers were capped and placed in a heating block overnight at 160 °C. After 24 h, beakers were uncapped and an additional 10 ml of $HClO_4$ was added. Samples were allowed to dry down, and were then treated with 12 ml of Aqua Regia (3:1 volume ratio HCl to HNO_3) and left in the heating block with the beakers capped for 4 h at 135 °C. The beakers were then uncapped and allowed to dry down overnight. When dry, samples were covered in 2 ml of 16 N HNO_3, allowed to dry down, and then suspended in 0.25 N HNO_3 solution.

A suite of 22 major and trace elements were measured in the suspended solutions via Inductively Coupled Plasma Atomic Emission Spectroscopy (ICP-AES) at the University of Washington Analytical Services Center. An internal standard was included in each run to assess the quality of the measurements. The standard deviation of 5 repeat measurements of the standard was <1 ppm for all elements. A full list of the elements measured, as well as the detection limits of each, can be found in Table S1. Major elements are reported as oxides.

For comparison, a suite of samples collected from BAS composite section D5.251 (Bowman et al., 2012; Bowman et al., 2014; Witts et al., 2016) was also analyzed for major and trace elements. These samples were collected by hand from shallow pits dug into the surface. Measurements of 9 major elements were made on 49 samples via X-ray fluorescence spectroscopy (XRF) at the University of Leicester, UK. Fusion beads were prepared from 2 to 3 g of bulk sediment and analyzed using a PANalytical Axios-Advanced XRF spectrometer. Results produced are in the form of weight percent of the component oxide adjusted for loss on ignition (LOI), which was determined prior to analysis by heating the samples in a furnace to 950 °C for 1–1.5 h. Although repeat analyses are not available, the relative standard deviation suggests a precision of better than 10%. A full list of elements measured, as well as LOI values, can be found in Table S2. Major elements are again reported as oxides.

Additional semi-quantitative analyses were conducted on 35 sediment samples from composite section D5.251 at the University of Leeds, UK using an Olympus Innovex 5000 Portable XRF (PXRF) in 'Soil mode' for comparison with T12 values. Samples were powdered using a mortar and pestle prior to analysis, and small amounts were placed in a container covered by a thin plastic film. Scan time was 154 s, and two analyses were made of each sample to check precision. Analyses were also checked using several international reference standards (CRM PACS-1, CRM MESS-2 and CRM STSD-3). A total of 28 major and trace elements were measured using this PXRF instrument.

Despite the semi-quantitative nature of these analyses, differences from reference standards were used to monitor accuracy, with any elements that deviated by more than ±30% from standard values removed from the final dataset ($n = 14$). One element (As) showed a + 37% error compared to one standard, but is included given that the remaining standards gave smaller errors. These errors appear large, but the PXRF dataset is primarily used as a screening technique, and trends are clearly comparable with XRF and ICP data even if absolute values differ (see below). Results are presented as ppm and converted to wt% oxides in the case of major elements (Table S3).

3.2. Carbon and sulfur geochemistry

A total of 48 bulk sediment samples taken from composite section D5.251 were analyzed for their total carbon (TC) and sulfur (TS) content using a LECO SC-144 DR analyzer at the University of Leeds. Relative Standard Deviation (%RSD) on these analyses is estimated at ±10%.

These same samples were also analyzed for their total organic carbon (TOC) content. Approximately 1 g of bulk sediment was weighed and then reacted for 24 h with ~5 ml of 10% HCl, to remove carbonate. Excess liquid was drawn off and the samples washed 3 times with milli-Q de-ionized water to remove residual acid and dissolved species. Samples were dried at 85 °C for 36 h, and reweighed to establish the mass of carbonate removed. 4-5 mg of this acid-washed sediment was then weighed out into tin cups and run in sequence with standards on a Micromass Isoprime continous flow mass spectrometer, coupled to a Eurovector or Elementar Pyrocube Elemental Analyser. Measured TOC was corrected to a proportion of the original sample mass prior to carbonate removal. Total Carbon (TC) was calculated from the corrected TOC and carbonate data. The precision obtained from repeat analysis of standard materials was <1 standard deviation.

To examine and quantify the amount of sulfur hosted by pyrite, extractions were carried out on 58 sediment samples from section D5.251, using the methodology of Poulton and Canfield (2005). Sulfides (in the form of H_2S) were liberated from 0.5–1 g of sediment and trapped as Ag_2S by reaction with $AgNO_3$. Pyrite S (wt%) was determined stoichiometrically from the original sample weight and weight of the precipitated Ag_2S. TOC and sulfur data are reported in Table S4.

3.3. Sedimentary microfacies and framboidal pyrite size distribution

To assess the overall mineralogy, composition, and presence of redox-sensitive minerals (primarily pyrite) in the LBF, a total of 33 sediment samples from section D5.251 were examined using an FEI Quanta 650 Scanning Electron Microscope (SEM) at the University of Leeds. This dataset expands on preliminary results presented by Witts et al. (2016). Bulk sediment samples ($n = 23$) were made into polished blocks by encasing several grams of sediment in resin. In addition, a set of powdered samples left over from analyses of sedimentary geochemistry ($n = 10$) were made into resin blocks and examined on the SEM. All polished blocks were carbon coated prior to SEM analysis, and quantitative mineralogy was determined using a built-in Oxford X-max 80 SDD EDS (Energy-dispersive X-ray spectroscope) and AZtec software.

The size distribution of pyrite framboids in both ancient and modern sediments has become a well-established proxy for local redox conditions, as framboid morphology is preserved even when sulfide

oxidation has altered the original chemical composition of the pyrite and surrounding sediment (Wilkin et al., 1996; Wignall and Newton, 1998; Bond and Wignall, 2010). Framboid analysis was conducted using a SEM, primarily in back-scatter mode. In most cases, 1–2 h were spent examining each block, and 100 framboids were counted. Samples containing fewer than 25 framboids likely do not provide statistically significant results, and are excluded from subsequent analysis, but are included in the Supplementary Material (Table S5).

4. Results

4.1. Major and trace element redox proxies

4.1.1. Molybdenum

The concentration of Mo in sediments is a versatile proxy for marine redox conditions. In typical, fully oxygenated marine waters, Mo concentrations in sediments reflect those of average continental crust, typically <5 ppm (Scott and Lyons, 2005). Enrichments are seen under suboxic conditions due to Mo complexing with manganese oxyhydroxides, which "shuttle" through soluble and insoluble phases across the oxic-anoxic interface. Under more intensely anoxic conditions, Mo can be strongly concentrated in sediments, as dissolved molybdate in the water column reacts with sulfide to form highly particle-reactive oxythiomolybdates (Tribovillard et al., 2006).

Molybdenum concentrations in the T12 section of the López de Bertodano Formation range from 21 to 144 ppm, with a mean of 51 ppm ($\sigma = 23$) and a median of 47 ppm (Fig. 2). As molybdenum in these sediments is enriched above typical crustal values, often by an order of magnitude or more, it likely represents authigenic deposition from seawater due to redox sensitive processes. Concentrations generally fall into the range identified by Scott and Lyons (2005) as representing suboxic to intermittently euxinic conditions. Values do occasionally impinge into the range of values (>80 ppm) indicative of pervasive euxinia, both in the lowermost part of the T12 section and around the K–Pg boundary.

In contrast, PXRF data from section D5.251 failed to detect Mo in any sediment samples, despite Mo levels in standard materials being in some cases overestimated by the instrument. This may result from the repeated oxidative weathering of the D5.251 surface samples by freeze-thaw processes. Furthermore, the loose sediments collected for section D5.251 may represent intervals of rapid sedimentation relative to the concretionary horizons collected for the T12 section, which would lead to less efficient accumulation of trace metals (see Section 5.1.1).

4.1.2. Iron and manganese

Manganese displays complex redox behavior, generally forming insoluble oxyhydroxides under oxidizing conditions and behaving as a soluble ion under reducing conditions. This may result in the "shuttling" of manganese across redox boundaries in the water column or sediments, a mechanism by which trace elements may be transferred to sediments and potentially retained (Tribovillard et al., 2006).

The mean MnO content of the T12 composite section is 0.46 wt%, with a minimum value of 0.05 wt% and a maximum of 2.26 wt% occurring in the lowermost part of the section (Fig. 2). MnO content was substantially lower in the D5.251 section, with values measured in fused samples via desktop XRF (Table S2) ranging from 0.02 to 0.68 wt%, with a mean value of 0.07 wt% and the maximum value occurring just above the K–Pg boundary. MnO content measured via PXRF (Table S3) shows similar patterns, with values ranging from 0.02 to 0.45 wt%, with a mean value of 0.05 wt%. This dataset was collected with a higher degree of resolution around two major glauconitic horizons, one at the K–Pg boundary, and another ~175 m below. Both show some degree of MnO enrichment, though the K–Pg horizon shows the highest values, at a single point (1009 m).

Like Mn, iron also shows complex "shuttling" behavior in environments with variable redox conditions. Insoluble iron oxyhydroxides can be dissolved in reducing porewaters, or as a result of chemocline fluctuations, and repeatedly transported to more distal parts of the basin, where they may be redeposited as oxyhydroxides or, if the deeper parts of the basin are euxinic, as sulfides. This authigenic enrichment of iron can best be traced in relation to aluminum, another metal common in terrigenous sediments, but one that is essentially diagenetically immobile (Lyons and Severmann, 2006).

Crossplots of Fe_2O_3 against Al_2O_3 show a clearly discernable detrital trend in both the T12 and D5.251sections (Fig. 3A). Enrichments in iron above this trend are attributed here to authigenic precipitation ($Fe_2O_{3\ auth}$). $Fe_2O_{3\ auth}$ has an average value of 4.37 wt%

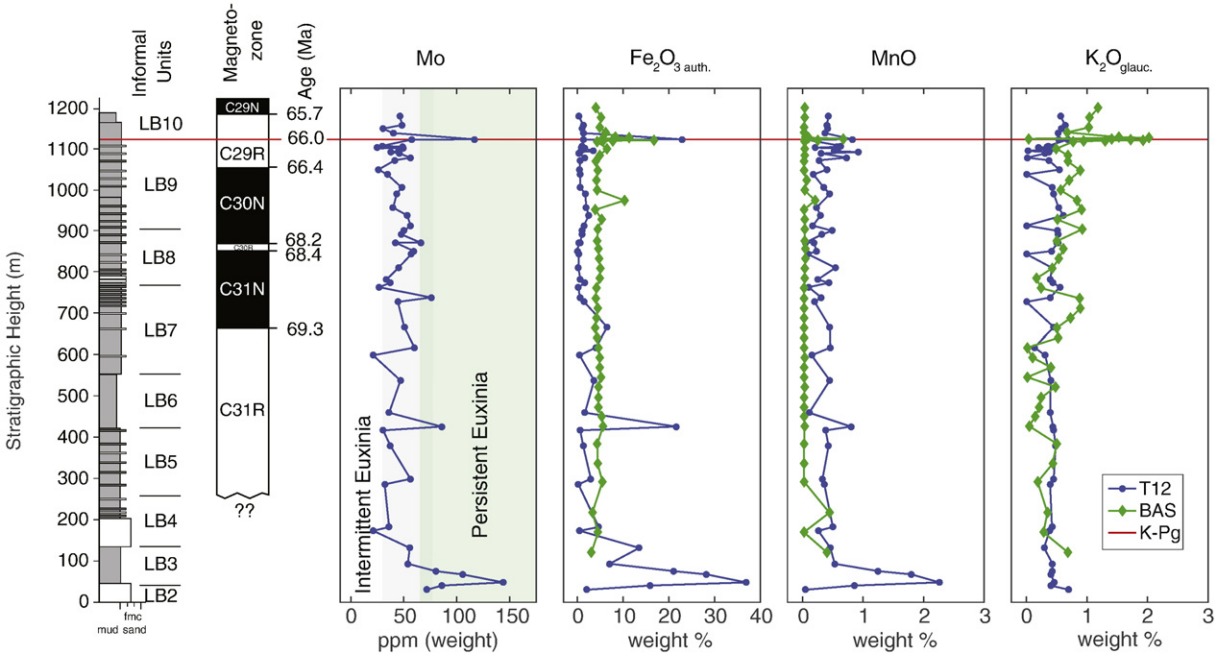

Fig. 2. Summary stratigraphy of Seymour Island sections with concentrations of Mo, authigenic Fe_2O_3, MnO, and glauconitic K_2O. LBX units are from Macellari (1988), magnetozones and interpreted ages are from Tobin et al. (2012). Authigenic Fe_2O_3 and glauconitic K_2O were determined based on crossplots in Fig. 3.

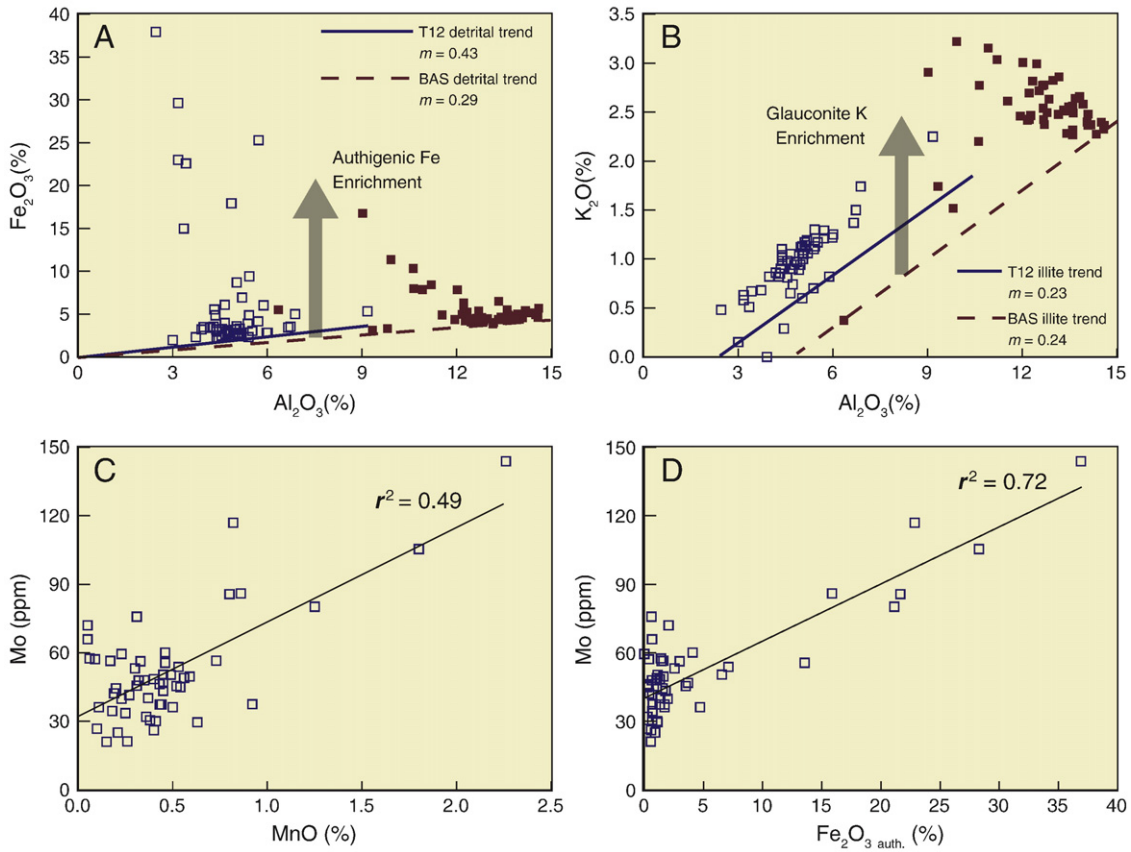

Fig. 3. Crossplots of major and trace elements in LBF strata. **A**: Al_2O_3 vs. Fe_2O_3, showing detrital trends and authigenic enrichments. **B**: Al_2O_3vs K_2O, showing inferred detrital trends and enrichments attributed to glauconite. **C**: MnO vs Mo in T12 section **D**: Authigenic Fe_2O_3 (from panel A) vs. Mo in T12 section. BAS refers to D5.251 composite section.

in the T12 composite section, with a maximum value of 36.90 wt% in the lower part of the section and another major peak (22.86 wt%) occurring at the K–Pg boundary. Authigenic Fe_2O_3 content was lower and less variable in the D5.251 section, with a mean value of 1.77 wt%, with the maximum value (14.09 wt%) occurring just below the K–Pg boundary. While Al was not measured in the PXRF dataset, absolute Fe_2O_3 values were highly consistent with measurements of fused samples (Tables S2–S3). Fe_2O_3 showed two maxima coincident with glauconitic horizons; one at the K–Pg boundary (max. = 16.41 wt%) and another of similar magnitude ~175 below (max = 16.68 wt%).

4.1.3. Other trace elements

Trace metals that can accumulate as cations in sulfide minerals (e.g., Cu, Zn, As, Cr) can serve as effective proxies for redox conditions if detrital sources for these elements can be excluded (Tribovillard et al., 2006). Several of these elements are present at significant concentrations in the T12 section and at significantly lower concentrations in the D5.251 section. Rather than instrumental inconsistencies, this likely reflects oxidation of sulfide minerals at the outcrop surface, where D5.251 samples were collected (see Section 5.1.1)

Zn concentrations in the T12 section range from 8.8 to 90.5 ppm, with a mean value of 43.2 ppm (Fig. 4). The highest values are seen in the lowermost *Rotularia* beds, though a local maximum (>60 ppm) is seen immediately prior to the K–Pg boundary. Cu shows relatively consistent values throughout the T12 section, ranging from 18.6 to 49.6 ppm, with a mean of 30.5 ppm. The highest values are seen ~30 below the K–Pg boundary. Cr shows consistent concentrations throughout the section, with the majority of values between 60 and 80 ppm, and no anomaly associated with the K–Pg boundary. A few higher (max. = 88.3 ppm) and lower (min. = 54.4 ppm) values are present, and the mean concentration is 68.3 ppm. Arsenic, which is strongly associated with sulfides, shows the largest range in concentration, from 145 to 670 ppm, with a mean value of 220 ppm. This dataset shows the most structure, with sporadic elevated values (>300 ppm) throughout the *Rotularia* beds, and a K–Pg boundary excursion reaching 472 ppm.

Zinc is one of the few trace metals that shows higher concentrations in the D5.251 section, where values range from 30.5 to 170.5 ppm, with a mean value of 71.5 ppm (Fig. 4). Zn content shows some secular decline from the '*Rotularia* Units to the 'Molluscan Units', but the prominent features of this record are two narrow intervals of Zn enrichment corresponding to the K–Pg boundary and another highly glauconitic interval ~175 m below. Cu is effectively absent from the D5.251 section, with no copper detected in most samples, and no values above 15 ppm. Cr shows a pattern similar to Zn, with two major peaks at the K–Pg boundary and the lower glauconitic interval. Values range from 12 to 118.5 ppm, with a mean of 72.6 ppm, which is consistent with the T12 section. Arsenic concentrations show some structure, with enrichments in the K–Pg and lower glauconitic intervals, but the absolute concentrations are substantially lower than those seen in the T12 section. Values range from 8.1 to 21.5 ppm, with a mean of 12.8 ppm.

4.2. Glauconite

Glauconite-rich horizons are observed in outcrop throughout the LBF (Macellari, 1988; Crame et al., 2004; Bowman et al., 2016), and are particularly prevalent in the uppermost ~300 m. Crossplots of potassium and aluminum abundance suggest that glauconite can be identified from major element data as an excess of K_2O not attributable to terrigenous clays (Fig. 3B). K_2O and Al_2O_3 show a strong positive correlation in many marine sedimentary systems, due to their common presence in illite-type clays (Shen et al., 2013). A detrital illite trend can be discerned in both datasets in Fig. 3B, with the similarity in slope suggesting a consistent illite composition. The presence of many points above this line indicates a secondary source of K_2O, one with a higher

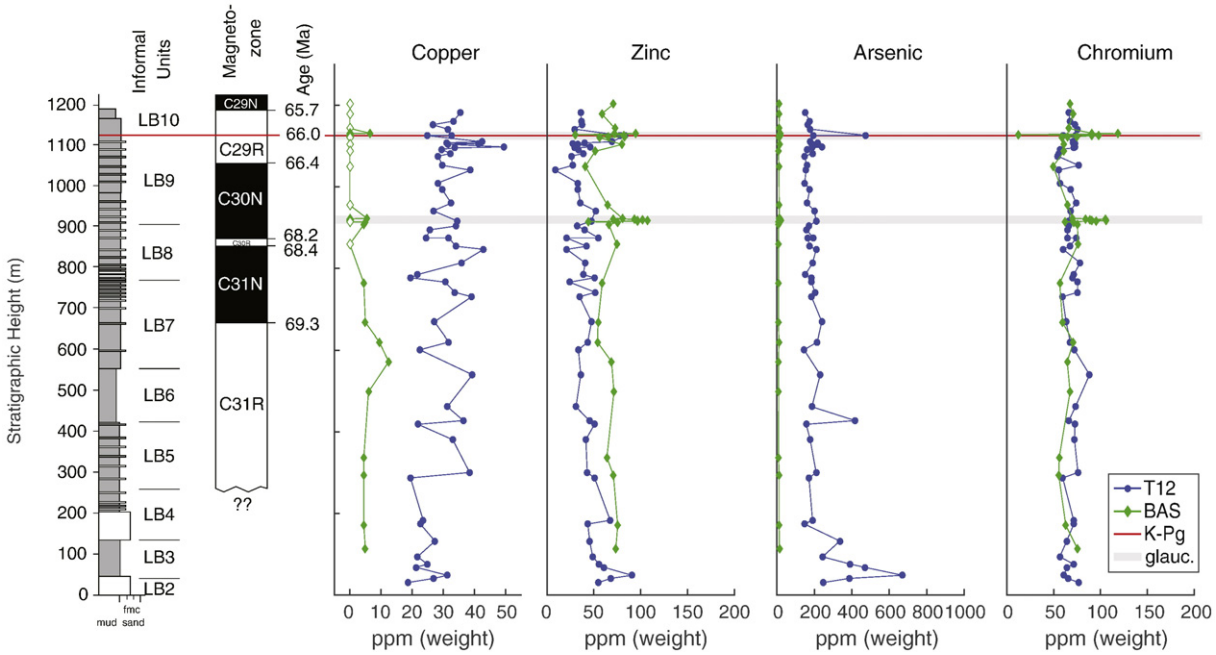

Fig. 4. Summary stratigraphy of Seymour Island sections with concentrations of Cu, Zn, As, and Cr. In Cu and As, concentrations were much higher in T12 samples, while concentrations of Zn and Cr were similar between sections. Values below the XRF detection limit (i.e., Cu in some BAS samples) are shown as zero. Gray shading represents prominent glauconitic intervals (however, note that these are not the only glauconitic horizons in the section).

K/Al ratio than illite, and field observations suggest this is likely to represent authigenic glauconite formation.

K_2O content attributable to authigenic glauconite (K_2O_{glauc}) averaged 0.39% ($\sigma = 0.17$) in the T12 section, with a maximum value of 0.70% in the lowermost sample and another local maximum (0.68%) coinciding with the K–Pg boundary (Fig. 2). A few samples appear to fall below the authigenic illite trend, possibly due to diagenetic alteration, and were assigned a K_2O_{glauc} value of 0. The D5.251 section, collected from southern Seymour Island, appears to be more glauconitic generally, with a mean K_2O_{glauc} value of 0.67% ($\sigma = 0.48$) and a maximum value of 2.02%, slightly above the K–Pg boundary. Some of this difference in K_2O_{glauc} content can likely be attributed to greater glauconite maturity in the D5.251 section, with the observed negative correlation between K_2O and Al_2O_3 being characteristic of glauconite evolution in siliciclastic sediments. Samples from the T12 section may contain less evolved glauconite, due to the selection of carbonate-cemented horizons during sample collection.

4.3. Carbon and sulfur species

The total organic carbon (TOC) content of the LBF is generally low (average of 0.37 wt%, maximum of 0.77 wt%, minimum of 0.14 wt%), consistent with previous measurements from the K–Pg boundary interval (Askin and Jacobson, 1989). Values are slightly higher (>0.5 wt%) in the lower and middle levels of the LBF (200–600 m in D5.251), with the remainder averaging between 0.2 and 0.5 wt% (Fig. 5). Total carbon (TC) is also generally low (average of 1.1 wt%, maximum of 6.23 wt%, minimum of 0.48 wt%). Several peaks in TC are evident in the lowermost LBF, and in the glauconite-rich K–Pg boundary interval, which may be due to concretionary calcite cements.

Total sulfur content ranges from 0.03 to 2.29 wt%, with an average of 0.42 wt% (Fig. 5). The highest values (>0.5 wt%) tend to occur in the lower and middle part of the succession (between 400 and 600 m). The remainder of the section is characterized by fluctuations between 0.1 and 1 wt%. The calculated weight percent of pyrite sulfur shows significantly lower values (average of 0.04 wt%, maximum of 0.23 wt%), with many samples recording values indistinguishable from 0. This is likely related to post-depositional oxidation of sulfides (see Section 5.1.1 below). As a result, the Total S data may partially reflect secondary sulfate minerals or sulfur bound to organic matter. The latter is perhaps less likely given the low TOC content.

4.4. Microfacies and framboidal pyrite

The pyrite population of the LBF can be divided into two main constituents; framboids, and euhedral pyrite (Fig. 6). Most framboids correspond to 'Type 1' as defined by Wignall and Newton (1998), being closely packed aggregations of uniformly-sized microcrysts. Rare 'Type 2' framboids and several large 'polyframboids' were also observed, and along with euhedral pyrite were not included in paleoredox interpretations due to their probable diagenetic origin (Wignall and Newton, 1998).

Pyrite framboid diameter data from the LBF are presented stratigraphically as box-and-whisker plots (Fig. 5), where the box encloses the range of the population, bounded by the 25th and 75th percentile, and whiskers define the extremes (minimum and maximum diameter) of the sample range (e.g. Wignall and Newton, 1998; Bond and Wignall, 2010). Out of a total of 33 blocks examined, most ($n = 21$) contained abundant framboids (>25 framboids identified), two samples contained very low numbers (<25 framboids identified), and 10 contained no identifiable framboids, euhedral pyrite, or evidence for weathered remnants of either.

A crossplot of mean framboid diameter versus standard deviation has also proved a useful method of assessing paleoredox conditions based on comparison with modern environments (Wilkin et al., 1996). 13 out of 21 LBF samples plot in the same field as data from modern euxinic settings (Fig. 7), whereas the remaining 8 plot closer to environments characterized by dysoxic conditions or high-frequency redox fluctuations. It is notable that most samples ($n = 16$), including several that plot in the euxinic field, contain a population of framboids with diameters >10 μm, with the size of this population ranging from 1 to nearly 20% in any given sample. The remaining samples ($n = 5$) contain only small framboids <10 μm in diameter, consistent with mostly syngenetic formation and the presence of sulfidic bottom waters below a redox boundary located in the water column.

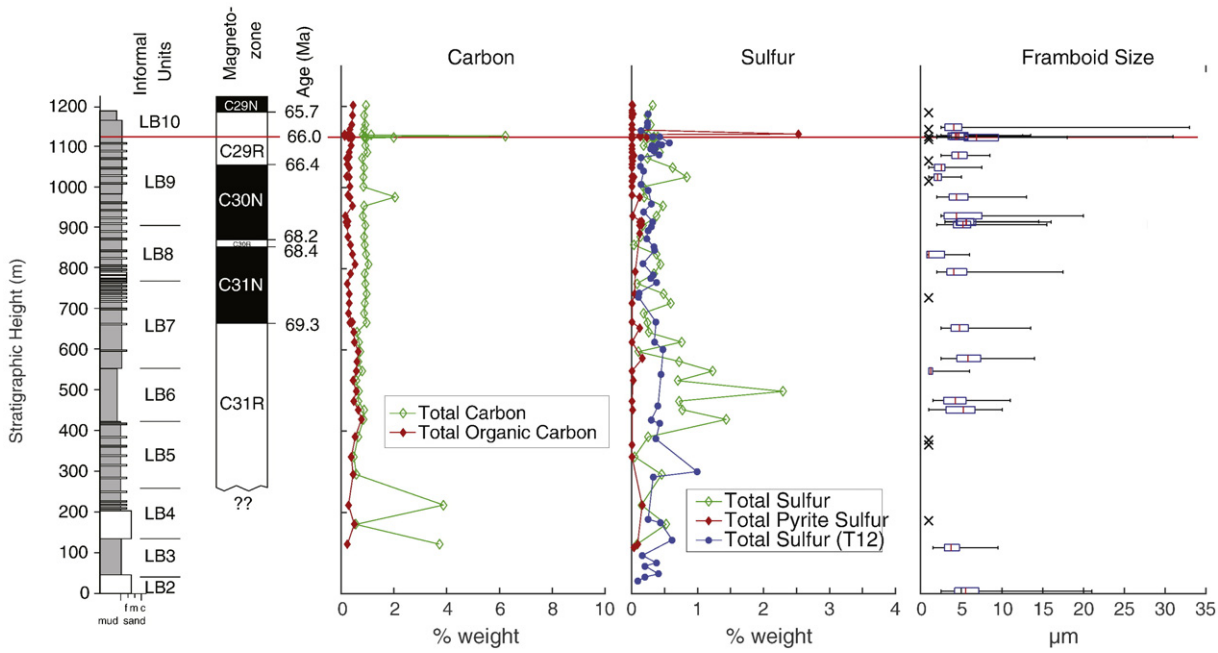

Fig. 5. Summary stratigraphy of Seymour Island sections with concentrations of carbon and sulfur, and framboid size distribution. All data are from BAS sections, with exception of sulfur concentrations from T12 (middle panel).

There are no clearly discernable stratigraphic trends in the framboid dataset. Witts et al. (2016) suggested that samples from close to the base of the LBF contained framboids with a smaller mean diameter and standard deviation, but in this expanded dataset this apparent correlation is weak. Samples containing no identifiable pyrite are usually considered oxic, and these are also spread throughout the section. Together the pyrite petrography suggests the LBF was characterized by rapid fluctuations in redox conditions.

It is notable that powdered samples ($n = 8$) exhibit the smallest mean framboid diameter and standard deviation, and these likely require a slightly different interpretive framework. Several ($n = 2$) are still equivocally non-euxinic in their size distribution. Several others ($n = 5$) plot in the euxinic field, though four of the five samples do not plot in the same range as any other LBF data or modern environments (Wilkin et al., 1996). This could indicate the loss of large framboids during crushing of the originally unconsolidated sediment samples. If this were the case, these samples are providing an erroneous picture of redox conditions. However, given the varied framboid size populations seen in other samples, and the time-averaged nature of polished blocks (see below), inclusion of powdered samples does not significantly change the overall interpretation of fluctuating redox conditions in the JRB.

5. Discussion

5.1. Controls on trace elements in the James Ross Basin

5.1.1. Evidence for oxidative weathering

Trace element data from the two transects show distinct differences, which require explanation before the signals can be interpreted as representing primary environmental conditions. Significant differences in the concentration of various elements between the two datasets are unlikely to be due to analytical error or the quantitative versus semi-quantitative nature of analyses in different laboratories. PXRF has been shown to be a valid method for detecting trace element enrichments to the same degree of accuracy and precision as ICP, if they are present in similar concentrations (Dahl et al., 2013). Instead, detailed comparison of the two datasets indicates that samples from section D5.251 are likely to have been affected by more intensive oxidative weathering than samples from section T12, leading to loss or non-detection of some trace elements.

Several trace elements (i.e., As, Cu) show considerably lower concentrations in section D5.251 compared to T12, while semi-quantitative PXRF analysis failed to detect any Mo or Ni in D5.251 samples, in contrast to the high concentrations of both elements found in the T12 section. All of these trace elements are commonly hosted in pyrite or other sulfide minerals, as well as organic matter (Huerta-Diaz and Morse, 1992; Large et al., 2014). Pyrite-S wt% values from section D5.251 are extremely low, despite the presence of pure (S-rich) framboids and diagenetic euhedral pyrite in microfacies samples. Microfacies work also revealed a significant amount of iron oxide present in many samples, in many cases visibly replacing both framboidal and euhedral pyrite, as would be expected during oxidative weathering. Concentrations of other trace elements (Zn, Cr) are more comparable between the two transects, indicating that while a component of these may be hosted in sulfides, they are also likely present in a silicate component.

An additional line of evidence for oxidation concerns the presence of sulfate minerals in the SI succession. In some places these form rusty-colored weathering 'crusts' on macrofossils, replacing molluscan shell material with blocky crystals of gypsum. Evidence for the retention of S during oxidative weathering can also be seen in crossplots of TOC vs. total S in samples from section D5.251 (Fig. 8A), where S/OC weight ratios range from values similar to those seen in typical Holocene anoxic sediments (~0.4; Dean and Arthur, 1989) up to values as high as 2.3. Because only a small fraction of Fe is in the form of pyrite (see Fig. 8B) and any organic carbon compounds remaining in surface-collected samples are likely to be highly refractory, the accumulation of sulfates can be traced on a normalized ternary diagram (Fig. 8C; Dean and Arthur, 1989; Rowe et al., 2008), where the samples define a trend of increasing relative S abundance corresponding to minimal change in the ratio of Fe to TOC. Although the abundance of sulfate minerals was not directly quantified, field observations indicate that this type of preservation is especially prevalent in the basal portion of the LBF on SI, which contains the highest concentrations of S in both transects.

These various lines of evidence suggest that trace elements were mobilized during oxidative weathering of sulfides, with samples from section D5.251, which were collected directly from the surface or from shallow pits, being especially affected. Sediment samples from the T12

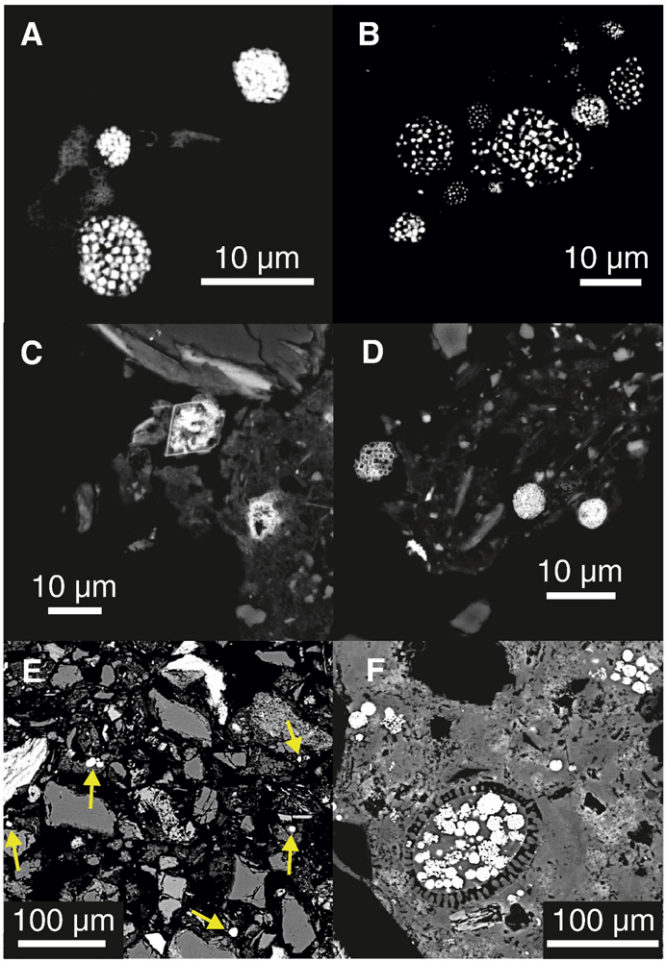

Fig. 6. Examples of pyrite morphologies encountered in section D5.251 through the LBF. **A**: (D5.481.1) Unweathered (FeS_2) syngenetic pyrite framboids, with regularly sized microcysts, indicative of formation in a euxinic water column. **B**: (D5.1108.1) Cluster of large, diagenetic framboids, indicative of prolonged growth within the sediment under anoxic conditions. Note variable microcryst sizes. **C:** (D5.1217.1) Relict euhedral (diagenetic) pyrite crystals, replaced by iron oxide. Associated with silicate (biotite, feldspar, and clay mineral) matrix. **D:** (D5.1243.1) Weathered (iron oxide) framboids showing characteristic 'hollow' appearance but retaining original size and morphology or microcrysts. **E:** (D5.406.1) General disposition of a typical sediment sample from the LBF, showing pyrite framboids (indicated by arrows) interspersed with fine-grained clastic grains (quartz, feldspars, biotite). **F:** (D5.1295.2) Mixture of diagenetic and syngenetic framboids (white objects) in glauconite-rich sample. Note that large diagenetic framboids are forming within regions formerly rich in organic material – in this case fish debris (large oval object in lower left of image) – located in the 'Fish-Kill' beds immediately above the K–Pg boundary (Zinsmeister, 1998). All images taken in back scatter electron mode.

section were collected from the ends of short (15–20 cm) cores, and may have escaped the most intense oxidative weathering occurring at the surface. Additionally, the T12 section preferentially targeted more indurated lithologies (Tobin et al., 2012), many of which contained a concretionary carbonate cement. The unconsolidated lithologies included in section D5.251 may have been more susceptible to freeze-thaw weathering and the removal of sulfide-hosted trace elements, in which case the T12 samples may be a better record of primary trace element concentrations at the time of deposition.

Changes in sedimentation rate may have also played a role, with intervals of slow deposition allowing greater concentrations of trace elements to accumulate in any given horizon. If the carbonate cementation of the T12 samples reflects intervals of slow sedimentation, then one would expect to see greater trace metal concentrations in these samples, even if the primary flux of trace elements from the water column to the sediments was the same for both sample sets. However, the origin of the

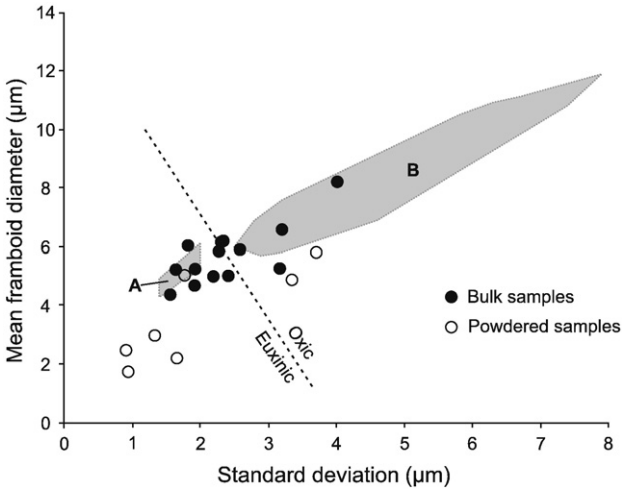

Fig. 7. Crossplot showing mean diameter (μm) vs. standard deviation (μm) of pyrite framboids from the López de Bertodano Formation on Seymour Island (section D5.251). Filled black circles are bulk sediment samples, open circles are powdered sediment samples. Dashed line is the boundary between oxic-dysoxic and anoxic-euxinic environments seen in modern depositional settings (taken from Wilkin et al., 1996). Shaded gray regions illustrate the range of size distributions and standard deviations of framboids from a range of modern euxinic (A) and dysoxic-oxic (B) settings (see Wilkin et al. (1996) for details).

concretionary cements is not clear, and this mechanism is probably not sufficient to explain the complete lack of Mo detected in section D5.251, which suggests that any Mo originally present was efficiently removed.

5.1.2. Relationship to glauconite horizons

A prominent feature of the trace and major element record is the apparent coincidence between enrichment in several trace elements (e.g., Cr, Zn, As) and glauconite-rich horizons in the LBF. This includes the K–Pg boundary and a prominent glauconite-rich interval located stratigraphically ~175 m below. Although no detailed sedimentological or geochemical work on glauconites from the LBF has been undertaken, preliminary work suggests that the glauconite in these intervals is autochthonous in origin (Bowman et al., 2016).

Glauconite typically forms in shelf settings at the sediment-water interface, and has been associated with low rates of terrigenous sediment input, localized reworking, and iron cycling (Amorosi, 1997; Amorosi et al., 2007). Such conditions are often associated with changing redox conditions in the sediment. This interpretation was followed by Macellari (1988), who interprets the glauconite-rich horizons in the LBF as representing chemical sedimentation during sea level highstands. Glauconite formation has also been observed in rapidly accumulating deltaic and shallow shelf environments in the modern ocean, where it is apparently linked with redox conditions; sediments collected from the Mississippi Delta region in the Gulf of Mexico at a present-day water depth of 29 m show a >2× increase in glauconite abundance coinciding with the expansion of hypoxic "dead zones" in the mid-20th century (Nelsen et al., 1994). Intervals of glauconite deposition were likely characterized by the local development of reducing bottom water conditions, and perhaps by transient lags in sedimentation, allowing for enhanced sulfide accumulation. They do not appear to be systematically associated with elevated TOC content, which may reflect poor TOC preservation at low sedimentation rates (Schoepfer et al., 2015)

5.2. Redox conditions during deposition of the LBF

5.2.1. Evidence for fluctuating redox conditions

Assuming the T12 section represents an accurate picture of elemental composition prior to weathering, the LBF contains significant enrichments in several redox-sensitive elements, indicative of deposition

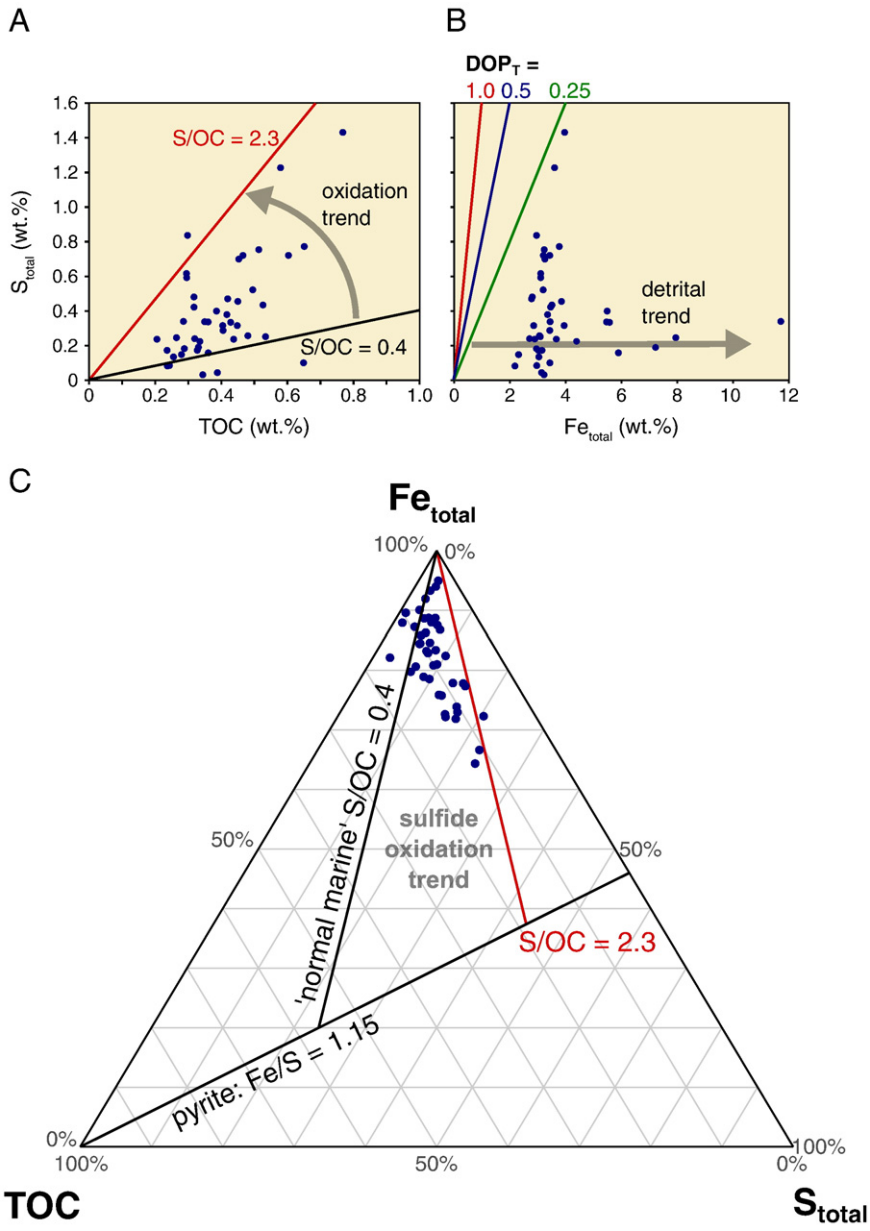

Fig. 8. Relationships between TOC, S, and Fe in samples from section D5.251 for which all three measurements are available. **A:** Crossplot of total organic carbon (wt%) vs. total sulfur (wt%). The S/OC ratio of 0.4 for 'normal marine' anoxic sediments is from Dean and Arthur (1989). **B:** Crossplot of total iron (wt%, as an element rather than an oxide) vs. total sulfur (wt%). S/Fe ratio lines correspond to 100%, 50%, and 25% pyritization of the total iron pool; note that all samples show a considerably lower degree of pyritization, and many samples show iron enrichments that are likely related to terrigenous content. **C:** Ternary diagram showing the normalized relative proportions of Fe_{total}, TOC, and S_{total}. Lines depicting the Fe/S ratio of pyrite and the S/OC ratio of 'normal marine' anoxic sediments are from Dean and Arthur (1989).

under at least intermittently euxinic conditions. This interpretation is supported by the abundance of small syndepositional (<6 μm) pyrite framboids in many sediment samples. The common presence of these alongside a framboid population with diameters >10 μm, and the sporadic occurrence of apparently oxic samples with no evidence for pyrite throughout the section, are indicative of dynamic changes in redox conditions, with the chemocline likely fluctuating across the sediment-water interface.

Trace element data provide additional support for this interpretation. Mo content shows a positive correlation with manganese content in the T12 dataset ($r^2 = 0.49$, $p = 5.6 \times 10^{-9}$, $n = 53$; Fig. 3C). Molybdenum is typically present at very low levels (<10 ppm) in sedimentary rocks deposited under oxic conditions (Scott and Lyons, 2012); the concentrations of molybdenum in Seymour Island sediments suggest suboxia and at least intermittent euxinia. Manganese, by contrast, is highly soluble under reducing conditions, and tends to accumulate in sediments only under oxic conditions (Tribovillard et al., 2006). The explanation for this apparent contradiction can be probably found in the role of manganese in "shuttling" other trace elements, including Mo, into the sediment in the form of oxyhydroxides, before dissolving under reducing conditions and diffusing back upward into the water column.

The positive correlation between MnO and Mo suggests that at least some manganese oxyhydroxides were retained in the sediments when molybdenum was deposited. Mo shows an even stronger positive correlation with authigenic iron ($r^2 = 0.72$, $p = 1.3 \times 10^{-15}$, $n = 53$; Fig. 3D), which like Mn is more soluble under reducing conditions and tends to shuttle across redox boundaries in the sediments or water column. However, unlike Mn, iron is more likely to be retained in anoxic sediments as sulfides (Tribovillard et al., 2006), which may explain its stronger relationship with Mo. Manganese concentrations are often highest just below the chemocline, where upward-diffusing Mn begins to

encounter dissolved oxygen and precipitate as oxyhydroxides (Tribovillard et al., 2006). If this boundary often existed at or near the sediment-water interface, or repeatedly fluctuated across the sediment surface, during deposition, it would explain how at least some Mn was retained in sediments during periods of Mo accumulation (Algeo and Tribovillard, 2009).

5.2.2. Dynamics of anoxia in the JRB

Having established the evidence for changes in redox conditions based on multiple proxies, it is important to consider the timescale of redox fluctuations recorded in the LBF. Although the mixed framboid population in most petrographic samples is consistent with rapid changes in bottom water redox conditions, the frequency of such fluctuations is beyond the observable resolution of the framboid dataset, due to the time-averaged nature of polished block samples collected at 1 m intervals. The temporal scale of redox fluctuations can potentially be estimated by examining the mechanisms of trace element enrichment, and comparing these to analogous modern environments, many of which are characterized by dynamic changes in redox conditions over short timescales (see Tyson and Pearson, 1991 for review).

A fluctuating chemocline, serving as a mechanism of both Mo and Fe-Mn oxyhydroxide enrichment in sediments, has been observed in several basins in the modern ocean, including Saanich Inlet, the Cariaco and Orca basins, and the Black Sea. While Fe-Mn oxyhydroxides do contribute to Mo enrichment in coastal upwelling zones (Zheng et al., 2000), persistently high Mo enrichments as a result of oxyhydroxide shuttling are generally a feature of "weakly restricted" environments (Algeo and Lyons, 2006; Algeo and Tribovillard, 2009). While the persistent restriction and euxinia of the Black Sea and the deep, hypersaline Orca Basin watermass make them poor analogues for the James Ross Basin, other modern environments may be more applicable.

The Cariaco Basin is a depression in the continental shelf north of Venezuela. Reaching maximum water depths around 1500 m, the basin is significantly deeper than the interpreted depositional environment of the López de Bertodano Formation. Deep waters are estimated to be approximately 50–100 years old (Algeo and Lyons, 2006), though several significant fluctuations in basinal redox conditions were observed over the 20th century (Zhang and Millero, 1993). This combination of decadal water renewal and oxyhydroxide shuttling yields authigenic Mo concentrations in the 50–200 ppm range (Dean et al., 1999; Algeo and Lyons, 2006) comparable to but generally higher than those seen in the James Ross Basin.

A better environmental analogue for the James Ross Basin might be Saanich Inlet, a fiord in Vancouver Island, British Columbia. With a maximum depth of approximately 200 m, and a significant freshwater and nutrient input from a 'point source' in the form of the Goldstream River, Saanich Inlet is more comparable to the inferred depositional environment of the López de Bertodano Formation (Olivero et al., 2007; Olivero, 2012). Deepwater renewal over semi-annual timescales leads to seasonable variability in the depth of the chemocline, leading to fluctuating redox conditions like those observed in sediments on Seymour Island. Sedimentary Mo concentrations range from ~20 to 120 ppm (Francois, 1988; Algeo and Lyons, 2006) comparable to the range seen in the López de Bertodano Formation.

Both of these environments are characterized by sills, however "particulate shuttle" like behavior has been observed in Mesozoic marine sediments not believed to be deposited in silled basins (Tribovillard et al., 2012). It is possible that slower circulation and greater density stratification during the Mesozoic led to restriction-like behavior even in relatively open marine environments. Manganese shuttling serves as a mechanism of Mo enrichment in unsilled (but increasingly eutrophic) Chesapeake Bay, during seasonal anoxic episodes, though the levels of authigenic Mo enrichment are considerably lower than those seen in the JRB (~5 ppm; Adelson et al., 2001). Mn shuttling between dissolved and particulate species has also been observed in Narragansett Bay (Graham et al., 1976), another unsilled estuary with seasonal anoxia.

Based on these comparisons, we propose that elemental enrichments in the James Ross Basin are most consistent with redox fluctuations on an approximately annual scale, which may be related to the intense seasonality of primary productivity imposed by the annual polar light cycle. The dynamic nature of redox fluctuations was likely controlled by the accumulation of nutrients draining from the forested highlands of the Antarctic Peninsula (Olivero et al., 2008; Bowman et al., 2014) and a seasonal pulse of productivity associated with the return of solar light in the polar spring, stimulating phytoplankton blooms. The utilization of this large standing supply of nutrients in the polar spring would have likely led to redox stratification of the water column, as decomposing plankton consumed the bottom water oxygen supply.

The samples shown in Fig. 8C show a range of S/OC and Fe/S ratios, as would be expected if pyrite formation was limited by the availability of labile organic carbon or sulfur rather than reactive iron (Dean and Arthur, 1989). Given the fully marine conditions and sulfate mineralization seen in parts of the section, the flux of organic carbon driving sulfate reduction was likely the factor limiting pyrite formation in these sediments.

Changing high-latitude climatic conditions during the Maastrichtian and Paleocene are evident based on data from the LBF on SI, potentially of sufficient magnitude to drive changes in redox. Large-scale blooms of the dinoflagellate cyst *Impletosphaeridium clavus* in the LBF have been linked to the decay of ephemeral sea ice during short-lived 'cold snaps' (Bowman et al., 2013) correlated to isotopic evidence for cool ocean temperatures (Tobin et al., 2012; Petersen et al., 2016). Others have suggested that these blooms are related to periods of higher continental nutrient influx and eutrophication, without the need to invoke sea ice formation (Amenábar et al., 2014). With or without sea ice, anoxic conditions were likely dynamically driven by seasonal bursts of high productivity, with their magnitude determined by the accumulation of a standing stock of dissolved nutrients during the polar winter. Trace element and framboid data do not show any significant evidence for enhanced levels of anoxia corresponding to dinoflagellate-rich intervals, which may suggest that they reflect preservation processes more than productivity.

Climate warming in the late Maastrichtian has also been suggested, based on faunal (Bowman et al., 2013; Bowman et al., 2014) and geochemical (Tobin et al., 2012; Petersen et al., 2016) proxies. An apparent peak in warming located in the ~70 m of the LBF stratigraphically below the K–Pg boundary, correlated to magnetochron C29R, has been linked to the main phase eruptions of the Deccan Traps LIP (Tobin et al., 2012; Renne et al., 2015; Petersen et al., 2016). Trace element and framboid data do not show any significant evidence for increased anoxia correlating with any of these events, suggesting that their impact on nutrient loading and/or bottom water oxygenation was not significant in this setting. Fluctuations in redox conditions seem to have been a characteristic feature of the JRB during the Maastrichtian and Paleocene, one that was not strongly perturbed by changes in climate.

5.3. Impact of anoxic conditions on Seymour Island fauna

The presence of a fully marine fauna in most of the LBF, despite evidence for at least periodically euxinic conditions in the sediment and bottom waters, does not necessarily represent a contradiction. Many modern environments that exhibit seasonal redox cyclicity host well-established benthic ecosystems (Tyson and Pearson, 1991; Oschmann, 1994). The degree to which changes in redox conditions prove deleterious for local marine biodiversity is governed by several factors, such as proximity to the source of nutrient inputs, the degree and timing of algal productivity, and the temporal and spatial extent of euxinic conditions. Apparent 'mismatches' between geochemical and paleontological proxies in environments deposited under conditions like those we postulate for the JRB are well known throughout the geological record (e.g. Kenig et al., 2004; Jiménez Berrocoso et al., 2008; Boyer et al., 2011), and

generally reflect the difference in the temporal scales recorded by macrofossils and trace element proxies.

Bivalve macrofossils from the LBF (e.g., *Lahillia*) exhibit well-preserved growth lines, which indicate they were on average 30–80 years old at death (J.L.O. Hall; Pers. Comm. 2016). This is consistent with analysis of similar bivalves of the genus *Cucullaea* from the younger La Meseta Formation on SI (Buick and Ivany, 2004), many of which lived >100 years. Rather than suggesting euxinia on decadal to centennial timescales, it is likely that the infaunal bivalve community was simply tolerant of short-lived euxinic events in the overlying water column. Indeed, bivalves can be quite resistant to short term anoxic and hypoxic conditions, particularly in cool water environments (Vaquer-Sunyer and Duarte, 2008).

Abundant benthic foraminifera have also been recovered from the LBF on Seymour Island (Huber, 1988) though interpretation of their oxygen tolerance is complicated. Several genera thought to be resistant to low oxygen conditions (Gupta and Machain-Castillo, 1993) are known throughout the LBF on Seymour Island, including *Bolivina* (3 species) and *Nonionella* (3 species). Regardless, periodic anoxic events on a seasonal scale are not necessarily in conflict with a diverse foraminiferal community that can reestablish itself quickly after oxic conditions return (Alve, 1995).

The degree of bioturbation is often considered to be a good indicator of the effects of redox changes on benthic fauna (e.g., Savrda and Bottjer, 1991). The LBF is often described as bioturbated throughout, and numerous specific ichnofossils have been identified from Seymour Island, as have areas of mottling inferred to be poorly defined bioturbation (Olivero and Cabrera, 2013). However, the recognition of the individual trace fossils (as opposed to intensive bioturbation), as well as the preservation of fine-scale sedimentary structures including current-ripple laminae, inclined heterolithic stratification, mudstone-sandstone couplets, and flaser bedding indicate that in at least some strata bioturbation was not significant (Olivero et al., 2007). Given the freeze-thaw weathering of surface sediments, and the necessity of locating or excavating fresh exposures to observe primary sedimentology, it is difficult to assess the relative abundance of bioturbation throughout the section. However, the presence of both extensively and minimally bioturbated intervals is consistent with our interpretation of frequent but short-lived periods of euxinia.

Apart from the mass extinction event at the K–Pg boundary itself, the most notable feature of the marine fossil record from the LBF on SI is an apparent long-term increase in the diversity and abundance of molluscan taxa up-section (Macellari, 1988; Crame et al., 2004; Witts et al., 2016). This increase is most pronounced in the transition between the mollusc-poor '*Rotularia* Units' and the overlying 'Molluscan Units' (which still contain abundant *Rotularia*; Macellari, 1988). Redox proxies examined here do not show a consistent change across this interval, implying that bottom water conditions were likely not the primary control on faunal diversity in these units. However, various lines of evidence suggest that more reducing conditions could have played at least a partial role in restricting diversity in the lower part of the section.

The stratigraphic interval corresponding to Units 2 through 4 (first ~250 m of the composite section presented here) contains the lowest overall macrofaunal diversity (Macellari, 1988; Witts et al., 2016). While framboid data are unfortunately too sparse to assess redox conditions at sufficient resolution, several samples are unequivocally euxinic (Fig. 5). The trace element dataset in this interval also contains some indications of more intense euxinia; the numerous local maxima in arsenic content in the T12 section likely reflect episodes of sulfide deposition in the *Rotularia* beds (Fig. 4). In a study of decapod crustaceans from the LBF, Feldmann and Tshudy (1989) noted morphological changes in the lower levels of the LBF, which they related to oxygen deficiency by comparison with modern taxa. This suggests that redox conditions had a substantial effect on the wider marine community in this interval.

This lowermost portion of the LBF on SI was deposited in shallower water, and was probably closer to the source of riverine nutrient and sediment input from the Antarctic Peninsula (Olivero et al., 2007; Olivero et al., 2008). This more proximal facies may have accumulated larger standing stocks of nutrients during the polar winter, leading to the local development of more intensely reducing conditions during spring phytoplankton blooms (as reflected in the stronger arsenic excursions seen in the *Rotularia* beds of section T12). It is likely that the increasing molluscan abundance up-section is a result of multiple factors relating to gradual deepening during the subsequent transgression (Olivero, 2012). This led to deposition in a more distal outer shelf setting further from the point-source for nutrient input, therefore further from the local development of more intense euxinia, as well as in water depths characterized by lower turbidity and less brackish conditions (Askin, 1988; Olivero et al., 2007). Other factors such as long-term changes in water temperature and nature of the available substrate likely also played a role in controlling diversity during the Maastrichtian–Paleocene deposition of the LBF (Witts et al., 2015; Witts et al., 2016).

In the 'cool-greenhouse' climate of latest-Cretaceous Antarctica, nutrient fluxes from the adjacent, vegetated landmass combined with the extreme seasonality of polar light regime (Chin et al., 2008) likely led to seasonal pulses of productivity, driving euxinia in the bottom waters of the shelf. The short duration and spatial heterogeneity of these redox changes could potentially be responsible for the superimposition of geochemical evidence for euxinia with a diverse macrofauna in these sections. In modern environments, benthic fauna can colonize the sea floor and tolerate periods of decreased oxygen content in the sediment or bottom water, providing that they do not persist long-term (typically >9 months-1 year; Tyson and Pearson, 1991; Oschmann, 1994; Vaquer-Sunyer and Duarte, 2008). It is certainly possible that the periods of euxinia identified from geochemical proxies may have led to mass mortality of benthic fauna, but corroborating this hypothesis would require high-resolution sampling of discreet stratigraphic intervals throughout the LBF linking paleontological, geochemical, and sedimentological proxies at the same scale.

5.4. A link between redox fluctuations and the K–Pg mass extinction in Antarctica?

An apparent peak in Mo concentration, and enrichments in other major and trace elements (Figs. 2,4), coincide with the K–Pg boundary as defined by biostratigraphy (Bowman et al., 2012), the presence of an Ir anomaly (Elliot et al., 1994), and mass extinction of marine taxa (Witts et al., 2016). It is tempting to link elemental enrichments at this level to environmental changes associated with the mass extinction, and by extension with the effects of the Chicxulub bolide impact (Kring, 2007; Schulte et al., 2010). Studies of redox-sensitive trace elements in other K–Pg boundary successions suggest a brief pulse of low oxygen conditions, and/or expansion of oxygen minimum zones, was associated with the aftermath of the impact, followed by a rapid recovery (over ~100 years) to pre-boundary conditions (Martinez-Ruiz et al., 1999; Sosa-Montes De Oca et al., 2013, 2017).

Major and trace element enrichments within the glauconite-rich beds at the K–Pg boundary on SI are similar to those seen in a separate glauconite-rich horizon, located approximately ~175 m below in section D5.251, one of several such intervals that occur throughout the section. Pyrite framboid size distributions are not significantly different between the two measured glauconite-rich horizons, with samples from both showing a low mean value but wide distribution of sizes, likely due to time-averaging of rapid redox variations. Despite its coincidence with the mass extinction event (Witts et al., 2016), the glauconite-rich horizon at the K–Pg boundary on SI is not appreciably different from others in the upper ~300 m of the LBF. The one unique characteristic of the K–Pg glauconite is the presence of abundant fish debris – including both articulated and disarticulated skeletons – in the few meters above the Ir anomaly (Zinsmeister, 1998; Witts et al., 2016).

In his original study of the K–Pg interval, Zinsmeister (1998) suggested that fossils in the 'fish-kill' beds were victims of unstable conditions in the water column following the Chicxulub impact and mass extinction (see also Witts et al., 2016). While such conditions may have included a short interval of intense euxinia, other factors related to a severe 'impact winter' (Vellekoop et al., 2016) and associated short-lived changes to climate and ocean mixing (Brugger et al., 2016) could be responsible for 'fish-kill' events in the JRB. Because of this uncertainty, and the similarities between enrichments at separate glauconite-rich horizons, it is not possible to unequivocally link the peak in Mo and other trace elements at the boundary with the environmental effects of the mass extinction. The more likely scenario is that any such signal is overprinted by the local geochemistry of this glauconite-rich horizon.

Based on the results presented in this study, a pulse of euxinia is unlikely to have been a significant kill mechanism during the K–Pg mass extinction in the JRB. Redox variations appear to have been a characteristic of the depositional environment, related to the unusual combination of a 'temperate' climate during the Cretaceous and Paleocene and the annual cycle of polar light availability. We did not detect any significant changes in the redox environment associated with the eruption of Deccan Traps LIP in the latest Cretaceous. Any redox changes in the aftermath of the Chicxulub impact were likely extremely short-lived (Sosa-Montes De Oca et al., 2013). Unlike other major mass extinction events in Earth history, the K–Pg crisis is not associated with a widespread expansion of anoxic or euxinic conditions in the oceans on a global scale (Wei et al., 2015; Wignall, 2015).

6. Conclusions

The succession on Seymour Island shows little secular variation over the studied Maastrichtian and earliest Danian interval. Based on several lines of geochemical and petrographic evidence, we can characterize the bottom water of the basin as intermittently euxinic, with periodic syngenetic framboid formation in the water column. Trace element enrichments appear to have been driven by manganese and iron oxyhydroxide "shuttling", which implies a fluctuating chemocline close to the sediment-water interface. Glauconite formation also appears to be related to redox variations, as well as sporadically slower sedimentation rates.

The LBF shows a similar degree of Mo enrichment to Saanich Inlet, which has deepwater turnover times on the order of one year. If anoxia in the JRB had a similar recurrence interval, it is likely related to a seasonal cycle of nutrient accumulation and productivity driven by the extreme seasonality of sunlight at polar latitudes even during periods of warm climate. As this anoxia would have been dynamically driven by primary productivity, its intensity would be proportional to the accumulation of nutrients in the water column during the polar winter.

Despite this evidence for euxinia, it does not appear to have been a major driver of marine diversity in the JRB. The limited diversity in the lowermost '*Rotularia* Units' may be attributable to more intensely reducing bottom water conditions, as evidenced by greater arsenic enrichments and a lower species richness in these strata. However, sporadic euxinia continued into the 'Molluscan Units', as benthic diversity increased. The K–Pg boundary horizon shows some trace element enrichments, but similar enrichments are also seen in other glauconitic intervals. Basinal euxinia does not appear to have increased coincident with Cretaceous climate changes, or the eruption of the main phase of the Deccan Traps. As a result it is likely to have been little more than a minor local contributor to the K–Pg mass extinction.

Acknowledgments

The authors would like to thank the staff of the University of Washington Analytic Services Center and Cohen Laboratories (School of Earth and Environment, University of Leeds, UK), as well as Robert Jamieson (University of Durham, UK), for laboratory support and assistance with major and trace element measurements. Fieldwork to Seymour Island to sample section D5.251 was funded by the UK Natural Environment Research Council (NERC) grant NE/C506399/1 (Antarctic Funding Initiative) and was supported logistically by the British Antarctic Survey. James Witts was funded by a PhD scholarship from the University of Leeds. Fieldwork to sample section T12 was funded by the U.S. National Science Foundation Office of Polar Programs (OPP-0739541, OPP-0739432), and supported logistically by the United States Antarctic Program, the crew of the *Laurence M. Gould*, and the Instituto Antártico Argentino. We thank Eduardo Olivero and Alvar Sobral for invaluable assistance in the field. We thank Peter Ward (University of Washington), Joseph Kirschvink (California Institute of Technology), Ross Mitchell (Yale University) Paul Wignall (University of Leeds), Jane Francis, Alistair Crame, and Vanessa Bowman (British Antarctic Survey), and Jon Ineson (GEUS, Denmark) for useful discussions and providing access to field samples.

Appendix A. Supplementary data

Supplementary data to this article can be found online at http://dx.doi.org/10.1016/j.palaeo.2017.04.013.

References

Adelson, J.M., Helz, G.R., Miller, C.V., 2001. Reconstructing the rise of recent coastal anoxia; molybdenum in Chesapeake Bay sediments. Geochim. Cosmochim. Acta 65 (2), 237–252.
Algeo, T.J., Lyons, T.W., 2006. Mo–total organic carbon covariation in modern anoxic marine environments: implications for analysis of paleoredox and paleohydrographic conditions. Paleoceanography 21 (1).
Algeo, T.J., Tribovillard, N., 2009. Environmental analysis of paleoceanographic systems based on molybdenum–uranium covariation. Chem. Geol. 268 (3), 211–225.
Alve, E., 1995. Benthic foraminiferal distribution and recolonization of formerly anoxic environments in Drammensfjord, southern Norway. Mar. Micropaleontol. 25 (2–3), 169–186.
Amenábar, C.R., Candel, M.S., Guerstein, G.R., 2014. Small Antarctic Late Cretaceous chorate dinoflagellate cysts: biological and palaeoenvironmental affinities. Palynology 38 (2), 303–323.
Amorosi, A., 1997. Detecting compositional, spatial, and temporal attributes of glaucony: a tool for provenance research. Sediment. Geol. 109 (1), 135–153.
Amorosi, A., Sammartino, I., Tateo, F., 2007. Evolution patterns of glaucony maturity: a mineralogical and geochemical approach. Deep-Sea Res. II Top. Stud. Oceanogr. 54 (11), 1364–1374.
Arens, N.C., West, I.D., 2008. Press-pulse: a general theory of mass extinction? Paleobiology 34 (04), 456–471.
Askin, R.A., 1988. The palynological record across the transition on Seymour Island, Antarctica. Geol. Soc. Am. Mem. 169, 155–162.
Askin, R.A., Jacobson, S.R., 1989. Total Organic Carbon Content and Rock Eval Pyrolysis on Outcrop Samples Across the Cretaceous/Tertiary Boundary, Seymour Island, Antarctica. 125(24) p. 123.
Bond, D.P., Wignall, P.B., 2010. Pyrite framboid study of marine Permian–Triassic boundary sections: a complex anoxic event and its relationship to contemporaneous mass extinction. Geol. Soc. Am. Bull. 122 (7–8), 1265–1279.
Bond, D.P., Wignall, P.B., 2014. Large igneous provinces and mass extinctions: an update. Geol. Soc. Am. Spec. Pap. 505 (pp. SPE505-02).
Boyer, D.L., Owens, J.D., Lyons, T.W., Droser, M.L., 2011. Joining forces: combined biological and geochemical proxies reveal a complex but refined high-resolution palaeo-oxygen history in Devonian epeiric seas. Palaeogeogr. Palaeoclimatol. Palaeoecol. 306 (3), 134–146.
Bowman, V.C., Francis, J.E., Riding, J.B., Hunter, S.J., Haywood, A.M., 2012. A latest Cretaceous to earliest Paleogene dinoflagellate cyst zonation from Antarctica, and implications for phytoprovincialism in the high southern latitudes. Rev. Palaeobot. Palynol. 171, 40–56.
Bowman, V.C., Francis, J.E., Riding, J.B., 2013. Late Cretaceous winter sea ice in Antarctica? Geology 41 (12), 1227–1230.
Bowman, V.C., Francis, J.E., Askin, R.A., Riding, J.B., Swindles, G.T., 2014. Latest Cretaceous–earliest Paleogene vegetation and climate change at the high southern latitudes: palynological evidence from Seymour Island, Antarctic Peninsula. Palaeogeogr. Palaeoclimatol. Palaeoecol. 408, 26–47.
Bowman, V., Ineson, J., Riding, J., Crame, J., Francis, J., Condon, D., Whittle, R., Ferraccioli, F., 2016. The Paleocene of Antarctica: Dinoflagellate cyst biostratigraphy, chronostratigraphy and implications for the palaeo-Pacific margin of Gondwana. Gondwana Res.
Brecher, H.H., Tope, R.W., 1988. Topographic map of Seymour Island. Geol. Soc. Am. Mem. 169, 17–20.
Brugger, J., Feulner, G., Petri, S., 2016. Baby, it's cold outside: climate model simulations of the effects of the asteroid impact at the end of the Cretaceous. Geophys. Res. Lett. 44. http://dx.doi.org/10.1002/2016GL072241.

Buick, D.P., Ivany, L.C., 2004. 100 years in the dark: extreme longevity of Eocene bivalves from Antarctica. Geology 32 (10), 921–924.

Caldeira, K.G., Rampino, M.R., 1990. Deccan volcanism, greenhouse warming, and the Cretaceous/Tertiary boundary. Geol. Soc. Am. Spec. Pap. 247, 117–124.

Chin, K., Bloch, J., Sweet, A., Tweet, J., Eberle, J., Cumbaa, S., Witkowski, J., Harwood, D., 2008. Life in a temperate Polar sea: a unique taphonomic window on the structure of a Late Cretaceous Arctic marine ecosystem. Proc. R. Soc. Lond. B Biol. Sci. 275 (1652), 2675–2685.

Clarke, L.J., Jenkyns, H.C., 1999. New oxygen isotope evidence for long-term Cretaceous climatic change in the Southern Hemisphere. Geology 27 (8), 699–702.

Courtillot, V., Fluteau, F., 2010. Cretaceous extinctions: the volcanic hypothesis. Science 328 (5981), 973–974.

Crame, J.A., Pirrie, D., Riding, J.B., Thomson, M.R.A., 1991. Campanian–Maastrichtian (Cretaceous) stratigraphy of the James Ross Island area, Antarctica. J. Geol. Soc. 148 (6), 1125–1140.

Crame, J.A., Francis, J.E., Cantrill, D.J., Pirrie, D., 2004. Maastrichtian stratigraphy of Antarctica. Cretac. Res. 25 (3), 411–423.

Crame, J.A., Pirrie, D., Riding, J.B., 2006. Mid-Cretaceous stratigraphy of the James Ross Basin, Antarctica. Geol. Soc. Lond., Spec. Publ. 258 (1), 7–19.

Dahl, T.W., Ruhl, M., Hammarlund, E.U., Canfield, D.E., Rosing, M.T., Bjerrum, C.J., 2013. Tracing euxinia by molybdenum concentrations in sediments using handheld X-ray fluorescence spectroscopy (HHXRF). Chem. Geol. 360, 241–251.

Davies, A., Kemp, A.E., Pike, J., 2009. Late Cretaceous seasonal ocean variability from the Arctic. Nature 460 (7252), 254–258.

Dean, W.E., Arthur, M.A., 1989. Iron-sulfur-carbon relationships in organic-carbon-rich sequences I: Cretaceous Western Interior Seaway. Am. J. Sci. 289 (6), 708–743.

Dean, W.E., Piper, D.Z., Peterson, L.C., 1999. Molybdenum accumulation in Cariaco basin sediment over the past 24 ky: a record of water-column anoxia and climate. Geology 27 (6), 507–510.

Ditchfield, P.W., Marshall, J.D., Pirrie, D., 1994. High latitude palaeotemperature variation: new data from the Thithonian to Eocene of James Ross Island, Antarctica. Palaeogeogr. Palaeoclimatol. Palaeoecol. 107 (1–2), 79–101.

Dutton, A., Huber, B.T., Lohmann, K.C., Zinsmeister, W.J., 2007. High-resolution stable isotope profiles of a dimitobelid belemnite: implications for paleodepth habitat and late Maastrichtian climate seasonality. PALAIOS 22 (6), 642–650.

Elliot, D.H., 1988. Tectonic setting and evolution of the James Ross Basin, northern Antarctic Peninsula. Geol. Soc. Am. Mem. 169, 541–556.

Elliot, D.H., Askin, R.A., Kyte, F.T., Zinsmeister, W.J., 1994. Iridium and dinocysts at the Cretaceous-Tertiary boundary on Seymour Island, Antarctica: implications for the KT event. Geology 22 (8), 675–678.

Feldmann, R.M., Tshudy, D.M., 1989. Evolutionary patterns in macrurous decapod crustaceans from Cretaceous to early Cenozoic rocks of the James Ross Island region, Antarctica. Geol. Soc. Lond., Spec. Publ. 47 (1), 183–195.

Feldmann, R.M., Woodburne, M.O. (Eds.), 1988. Geology and Paleontology of Seymour Island, Antarctic Peninsula. vol. 169. Geological Society of America.

Francois, R., 1988. A study on the regulation of the concentrations of some trace metals (Rb, Sr, Zn, Pb, Cu, V, Cr, Ni, Mn and Mo) in Saanich Inlet sediments, British Columbia, Canada. Mar. Geol. 83 (1), 285–308.

Friedrich, O., Norris, R.D., Erbacher, J., 2012. Evolution of middle to Late Cretaceous oceans—a 55 my record of Earth's temperature and carbon cycle. Geology 40 (2), 107–110.

Graham, W.F., Bender, M.L., Klinkhammer, G.P., 1976. Manganese in Narragansett Bay. Limnol. Oceanogr. 21 (5), 665–673.

Gupta, B.K.S., Machain-Castillo, M.L., 1993. Benthic foraminifera in oxygen-poor habitats. Mar. Micropaleontol. 20 (3–4), 183–201.

Hathway, B., 2000. Continental rift to back-arc basin: Jurassic–Cretaceous stratigraphical and structural evolution of the Larsen Basin, Antarctic Peninsula. J. Geol. Soc. 157 (2), 417–432.

Huber, B.T., 1988. Upper Campanian-Paleocene foraminifera from the James Ross Island region, Antarctic Peninsula. Geol. Soc. Am. Mem. 169, 163–252.

Huerta-Diaz, M.A., Morse, J.W., 1992. Pyritization of trace metals in anoxic marine sediments. Geochim. Cosmochim. Acta 56 (7), 2681–2702.

Jiménez Berrocoso, Á., MacLeod, K.G., Calvert, S.E., Elorza, J., 2008. Bottom water anoxia, inoceramid colonization, and benthopelagic coupling during black shale deposition on Demerara Rise (Late Cretaceous western tropical North Atlantic). Paleoceanography 23 (3).

Kenig, F., Hudson, J.D., Damsté, J.S.S., Popp, B.N., 2004. Intermittent euxinia: reconciliation of a Jurassic black shale with its biofacies. Geology 32 (5), 421–424.

Kidder, D.L., Worsley, T.R., 2010. Phanerozoic large igneous provinces (LIPs), HEATT (haline euxinic acidic thermal transgression) episodes, and mass extinctions. Palaeogeogr. Palaeoclimatol. Palaeoecol. 295 (1), 162–191.

Kilian, W., Reboul, P., 1909. Les céphalopodes neocretaces des iles Seymour et Snow-Hill. Wissenschaftliche Ergebnisse der Schwedischen Siidpolar-Expedition 1901–1903, Stockholm. vol. 3 (6) pp. 1–75.

Kring, D.A., 2007. The Chicxulub impact event and its environmental consequences at the Cretaceous–Tertiary boundary. Palaeogeogr. Palaeoclimatol. Palaeoecol. 255 (1), 4–21.

Large, R.R., Halpin, J.A., Danyushevsky, L.V., Maslennikov, V.V., Bull, S.W., Long, J.A., Gregory, D.D., Lounejeva, E., Lyons, T.W., Sack, P.J., McGoldrick, P.J., 2014. Trace element content of sedimentary pyrite as a new proxy for deep-time ocean–atmosphere evolution. Earth Planet. Sci. Lett. 389, 209–220.

Lawver, L.A., Gahagan, L.M., Coffin, M.F., 1992. The Development of paleoseaways Around Antarctica. The Antarctic Paleoenvironment: A PERSPECTIVE on Global Change: Part One. pp. 7–30.

Linnert, C., Robinson, S.A., Lees, J.A., Bown, P.R., Pérez-Rodríguez, I., Petrizzo, M.R., Falzoni, F., Littler, K., Arz, J.A., Russell, E.E., 2014. Evidence for global cooling in the Late Cretaceous. Nat. Commun. 5.

Lyons, T.W., Severmann, S., 2006. A critical look at iron paleoredox proxies: new insights from modern euxinic marine basins. Geochim. Cosmochim. Acta 70 (23), 5698–5722.

Macellari, C.E., 1986. Late Campanian-Maastrichtian ammonite fauna from Seymour Island (Antarctic Peninsula). Memoir 1–55.

Macellari, C.E., 1988. Stratigraphy, sedimentology, and paleoecology of Upper Cretaceous/Paleocene shelf-deltaic sediments of Seymour Island. Geol. Soc. Am. Mem. 169, 25–54.

Martinez-Ruiz, F., Ortega-Huertas, M., Palomo, I., 1999. Positive Eu anomaly development during diagenesis of the K/T boundary ejecta layer in the Agost section (SE Spain): implications for trace-element remobilization. Terra Nova 11 (6), 290–296.

McArthur, J.M., Thirlwall, M.F., Engkilde, M., Zinsmeister, W.J., Howarth, R.J., 1998. Strontium isotope profiles across K/T boundary sequences in Denmark and Antarctica. Earth Planet. Sci. Lett. 160 (1), 179–192.

McArthur, J.M., Crame, J.A., Thirlwall, M.F., 2000. Definition of Late Cretaceous stage boundaries in Antarctica using strontium isotope stratigraphy. J. Geol. 108 (6), 623–640.

Miller, K.G., Kominz, M.A., Browning, J.V., Wright, J.D., Mountain, G.S., Katz, M.E., Sugarman, P.J., Cramer, B.S., Christie-Blick, N., Pekar, S.F., 2005. The Phanerozoic record of global sea-level change. Science 310 (5752), 1293–1298.

Montes, M., Nozal, F., Santillana, S., Marenssi, S. and Olivero, E., 2013. Mapa Geológico de la isla Marambio (Seymour) Escala 1: 20.000. Serie Cartográfica Geocientífica Antártica.

Nelsen, T.A., Blackwelder, P., Hood, T., McKee, B., Romer, N., Alvarez-Zarikian, C., Metz, S., 1994. Time-based correlation of biogenic, lithogenic and authigenic sediment components with anthropogenic inputs in the Gulf of Mexico NECOP study area. Estuaries 17 (4), 873–885.

Olivero, E.B., 1998. Large mud-filled channels in the Maastrichtian of the López de Bertodano Formation (Seymour Island, Antarctica): stratigraphical implications. Rev. Asoc. Geol. Argent. 53 (4), 553–556.

Olivero, E.B., 2012. Sedimentary cycles, ammonite diversity and palaeoenvironmental changes in the Upper Cretaceous Marambio Group, Antarctica. Cretac. Res. 34, 348–366.

Olivero, E.B., Cabrera, M.I.L., 2013. *Euflabella* n. igen.: complex horizontal spreite burrows in Upper Cretaceous–Paleogene shallow-marine sandstones of Antarctica and Tierra del Fuego. J. Paleontol. 87 (3), 413–426.

Olivero, E.B., Ponce, J.J., Marsicano, C.A., Martinioni, D.R., 2007. Depositional settings of the basal López de Bertodano formation, Maastrichtian, Antarctica. Rev. Asoc. Geol. Argent. 62 (4), 521–529.

Olivero, E.B., Ponce, J.J., Martinioni, D.R., 2008. Sedimentology and architecture of sharp-based tidal sandstones in the upper Marambio Group, Maastrichtian of Antarctica. Sediment. Geol. 210 (1), 11–26.

Oschmann, W., 1994. Adaptive pathways of benthic organisms in marine oxygen-controlled environments (with 14 figures in the text). Neues Jb. Geol. Paläontol. Abh. 191 (3), 393–444.

Petersen, S.V., Dutton, A., Lohmann, K.C., 2016. End-Cretaceous extinction in Antarctica linked to both Deccan volcanism and meteorite impact via climate change. Nat. Commun. 7.

Pirrie, D., Crame, J.A., Lomas, S.A., Riding, J.B., 1997. Late Cretaceous stratigraphy of the admiralty sound region, James Ross Basin, Antarctica. Cretac. Res. 18 (1), 109–137.

Poulton, S.W., Canfield, D.E., 2005. Development of a sequential extraction procedure for iron: implications for iron partitioning in continentally derived particulates. Chem. Geol. 214 (3), 209–221.

Renne, P.R., Sprain, C.J., Richards, M.A., Self, S., Vanderkluysen, L., Pande, K., 2015. State shift in Deccan volcanism at the Cretaceous-Paleogene boundary, possibly induced by impact. Science 350 (6256), 76–78.

Riding, J.B., Crame, J.A., 2002. Aptian to Coniacian (Early–Late Cretaceous) palynostratigraphy of the Gustav Group, James Ross Basin, Antarctica. Cretac. Res. 23 (6), 739–760.

Rinaldi, C.A., Massabie, A., Morelli, J., Rosenman, H.L., Del Valle, R., 1978. Geologia de la isla Vicecomodoro Marambio. Contrib. Inst. Antart. Argent. 217, 1–37.

Rowe, H.D., Loucks, R.G., Ruppel, S.C., Rimmer, S.M., 2008. Mississippian Barnett Formation, Fort Worth Basin, Texas: bulk geochemical inferences and Mo–TOC constraints on the severity of hydrographic restriction. Chem. Geol. 257 (1), 16–25.

Savrda, C.E., Bottjer, D.J., 1991. Oxygen-related biofacies in marine strata: an overview and update. Geol. Soc. Lond., Spec. Publ. 58 (1), 201–219.

Schoene, B., Samperton, K.M., Eddy, M.P., Keller, G., Adatte, T., Bowring, S.A., Khadri, S.F., Gertsch, B., 2015. U-Pb geochronology of the Deccan Traps and relation to the end-Cretaceous mass extinction. Science 347 (6218), 182–184.

Schoepfer, S.D., Shen, J., Wei, H., Tyson, R.V., Ingall, E., Algeo, T.J., 2015. Total organic carbon, organic phosphorus, and biogenic barium fluxes as proxies for paleomarine productivity. Earth Sci. Rev. 149, 23–52.

Schulte, P., Alegret, L., Arenillas, I., Arz, J.A., Barton, P.J., Bown, P.R., Bralower, T.J., Christeson, G.L., Claeys, P., Cockell, C.S., Collins, G.S., 2010. The Chicxulub asteroid impact and mass extinction at the Cretaceous-Paleogene boundary. Science 327 (5970), 1214–1218.

Scott, C., Lyons, T., 2005. Defining an uniquely euxinic molybdenum signal. Geochim. Cosmochim. Acta 69, 577.

Scott, C., Lyons, T.W., 2012. Contrasting molybdenum cycling and isotopic properties in euxinic versus non-euxinic sediments and sedimentary rocks: refining the paleoproxies. Chem. Geol. 324, 19–27.

Shen, J., Algeo, T.J., Hu, Q., Xu, G., Zhou, L., Feng, Q., 2013. Volcanism in South China during the Late Permian and its relationship to marine ecosystem and environmental changes. Glob. Planet. Chang. 105, 121–134.

Smellie, J.L., Johnson, J.S., McIntosh, W.C., Esser, R., Gudmundsson, M.T., Hambrey, M.J., De Vries, B.V.W., 2008. Six million years of glacial history recorded in volcanic lithofacies of the James Ross Island Volcanic Group, Antarctic Peninsula. Palaeogeogr. Palaeoclimatol. Palaeoecol. 260 (1), 122–148.

Sosa-Montes De Oca, C., Martínez-Ruiz, F., Rodríguez-Tovar, F.J., 2013. Bottom-water conditions in a marine basin after the Cretaceous–Paleogene impact event: timing the recovery of oxygen levels and productivity. PLoS One 8 (12), e82242.

Sosa-Montes De Oca, C.S.M., Rodríguez-Tovar, F.J., Martínez-Ruiz, F., Monaco, P., 2017. Paleoenvironmental conditions across the Cretaceous–Paleogene transition at the Apennines sections (Italy): an integrated geochemical and ichnological approach. Cretac. Res. 71, 1–13.

Spath, L.F., 1953. The Upper Cretaceous cephalopod fauna of Graham Land. Falkland Island Dependencies Survey Scientific Report. vol. 3, pp. 1–60.

Svojtka, M., Nývlt, D., Murakami, M., Vávrová, J., Filip, J., Mixa, P., 2009. Provenance and post-depositional low-temperature evolution of the James Ross Basin sedimentary rocks (Antarctic Peninsula) based on fission track analysis. Antarct. Sci. 21 (06), 593–607.

Tobin, T.S., Ward, P.D., 2015. Carbon isotope ($\delta^{13}C$) differences between Late Cretaceous ammonites and benthic mollusks from Antarctica. Palaeogeogr. Palaeoclimatol. Palaeoecol. 428, 50–57.

Tobin, T.S., Ward, P.D., Steig, E.J., Olivero, E.B., Hilburn, I.A., Mitchell, R.N., Diamond, M.R., Raub, T.D., Kirschvink, J.L., 2012. Extinction patterns, $\delta^{18}O$ trends, and magnetostratigraphy from a southern high-latitude Cretaceous–Paleogene section: links with Deccan volcanism. Palaeogeogr. Palaeoclimatol. Palaeoecol. 350, 180–188.

Tobin, T.S., Bitz, C.M., Archer, D., 2016. Modeling climatic effects of carbon dioxide emissions from Deccan Traps volcanic eruptions around the Cretaceous–Paleogene boundary. Palaeogeogr. Palaeoclimatol. Palaeoecol. http://dx.doi.org/10.1016/j.palaeo.2016.05.028.

Tribovillard, N., Algeo, T.J., Lyons, T., Riboulleau, A., 2006. Trace metals as paleoredox and paleoproductivity proxies: an update. Chem. Geol. 232 (1), 12–32.

Tribovillard, N., Algeo, T.J., Baudin, F., Riboulleau, A., 2012. Analysis of marine environmental conditions based on molybdenum–uranium covariation—applications to Mesozoic paleoceanography. Chem. Geol. 324, 46–58.

Tyson, R.V., Pearson, T.H., 1991. Modern and ancient continental shelf anoxia: an overview. In: Tyson, R.V., Pearson, T.H. (Eds.), Geological Society of London Special Publication. vol. 58, pp. 1–24.

Vaquer-Sunyer, R., Duarte, C.M., 2008. Thresholds of hypoxia for marine biodiversity. Proc. Natl. Acad. Sci. 105 (40), 15452–15457.

Vellekoop, J., Esmeray-Senlet, S., Miller, K.G., Browning, J.V., Sluijs, A., van de Schootbrugge, B., Damsté, J.S.S., Brinkhuis, H., 2016. Evidence for Cretaceous-Paleogene boundary bolide "impact winter" conditions from New Jersey, USA. Geology 44 (8), 619–622.

Wei, H., Shen, J., Schoepfer, S.D., Krystyn, L., Richoz, S., Algeo, T.J., 2015. Environmental controls on marine ecosystem recovery following mass extinctions, with an example from the Early Triassic. Earth Sci. Rev. 149, 108–135.

Wignall, P.B., 2001. Large igneous provinces and mass extinctions. Earth Sci. Rev. 53 (1), 1–33.

Wignall, P.B., 2015. The Worst of Times: How Life on Earth Survived Eighty Million Years of Extinctions. Princeton University Press.

Wignall, P.B., Newton, R., 1998. Pyrite framboid diameter as a measure of oxygen deficiency in ancient mudrocks. Am. J. Sci. 298 (7), 537–552.

Wilckens, O., 1910. Die Anneliden, Bivalven und Gastropoden der Antarktischen Kreideformation. Wissenschaftliche Ergebnisse der Schwedischen Siidpolar-Expedition 1901–1903, Stockholm. vol. 3(12) pp. 1–132.

Wilkin, R.T., Barnes, H.L., Brantley, S.L., 1996. The size distribution of framboidal pyrite in modern sediments: an indicator of redox conditions. Geochim. Cosmochim. Acta 60 (20), 3897–3912.

Witts, J.D., Bowman, V.C., Wignall, P.B., Crame, J.A., Francis, J.E., Newton, R.J., 2015. Evolution and extinction of Maastrichtian (Late Cretaceous) cephalopods from the López de Bertodano Formation, Seymour Island, Antarctica. Palaeogeogr. Palaeoclimatol. Palaeoecol. 418, 193–212.

Witts, J.D., Whittle, R.J., Wignall, P.B., Crame, J.A., Francis, J.E., Newton, R.J., Bowman, V.C., 2016. Macrofossil evidence for a rapid and severe Cretaceous-Paleogene mass extinction in Antarctica. Nat. Commun. 7.

Zhang, J.Z., Millero, F.J., 1993. The chemistry of the anoxic waters in the Cariaco Trench. Deep-Sea Res. I Oceanogr. Res. Pap. 40 (5), 1023–1041.

Zheng, Y., Anderson, R.F., van Geen, A., Kuwabara, J., 2000. Authigenic molybdenum formation in marine sediments: a link to pore water sulfide in the Santa Barbara Basin. Geochim. Cosmochim. Acta 64 (24), 4165–4178.

Zinsmeister, W.J., 1998. Discovery of fish mortality horizon at the KT boundary on Seymour Island: re-evaluation of events at the end of the Cretaceous. J. Paleontol. 72 (03), 556–571.

Zinsmeister, W.J., 2001. Late Maastrichtian short-term biotic events on Seymour Island, Antarctic Peninsula. J. Geol. 109 (2), 213–229.